STRUCTURAL, MORPHOLOGICAL AND OPTICAL PROPERTIES OF ZnO NANOPARTICLE DOPED BY MANGANESE (Mn) AND GADOLIUM (Gd) AND ITS ANTIMICROBIAL ACTIVITY USING CO-PRECIPITATION METHOD

BY

DIRIBA TSEGAYE RETA

A THESIS SUBMITTED TO APPLIED PHYSICS PROGRAM

SCHOOL OF APPLIED NATURAL SCIENCE

OFFICE OF GRADUATE STUDIES

July, 2020

Adama, Ethiopia

STRUCTURAL, MORPHOLOGICAL AND OPTICAL PROPERTIES OF ZnO NANOPARTICLE DOPED BY MANGANESE (Mn) AND GADOLIUM (Gd) AND ITS ANTIMICROBIAL ACTIVITY USING CO-PRECIPITATION METHOD

BY

DIRIBA TSEGAYE RETA

ADVISOR: Dr. ABEBE BELAY GEMTA

A THESIS SUBMITTED TO APPLIED PHYSICS PROGRAM
SCHOOL OF APPLIED NATURAL SCIENCE
OFFICE OF GRADUATE STUDIES

ADAMA SCIENCE AND TECHNOLOGY UNIVERSITY

July, 2020
Adama, Ethiopia

Approval Page

We the undersigned members of the Board of Examiners of the Final open defense by **DIRIBA TSEGAYE RETA** have read and evaluated his thesis entitled "**STRUCTURAL, OPTICAL AND MORPHOLOGICAL PROPERTIES OF ZNO NANOPARTICLE DOPED BY MANGANESE (MN) AND GADOLLIUM (GD) AND ITS ANTI-MICROBIAL ACTIVITY USING CO –PRECIPITATION METHOD**" and examined the candidate. This is therefore to certify that the thesis has been accepted in partial fulfillment of the requirement of the **Degree of Master of Master of Science in Applied Physics (Laser Spectroscopy).**

Name	Signature	Date
Diriba Tsegaye		21/07/2020
Name of Student		
Dr. ABEBE BELAY		23/07/2020
Advisor		
Dr. MEGERSA WODAJO		23/07/2020
Internal Examiner		
Dr. CHERNET AMENTE		23/07/2020
External Examiner		
Dr. ANNO KARE		23/07/2020
Chairman አኖ ካሬ አኖ (ዶ/ር) Anno Kare Anno (Ph D)		24/07/2020
Department Head ተገኔ ደሳለኝ ዘለቀ (ዶ/ር) Tegene Desalegn Zeleke (PhD)		17/08/2020
School Dean (SoANS) ለገሠ ለሜቻ ኦሱ (ፒኤች ዲ) Legesse Lemecha Obsu (PhD)		17/08/20
Post Graduate Dean		

Declaration

I hereby declare that this MSc.thesis is my original work and has not been presented for a degree in any other university, and all sources of material used for this thesis have been duly acknowledged.

Name: Diriba Tsegaye

Signature:_____

This MSc. thesis has been submitted for examination with our approval as thesis advisors.

Advisor Name: Abebe Belay (PhD)

Signature:_____

Date of submission:_____

Acknowledgements

First of all, I would like to express my gratitude to my advisor Dr. Abebe Belay for his endless guidance, most support, motivation, encouragement, and patient help during my research work. He kindly read this thesis and offered invaluable detailed advices on organization and the theme of the thesis. This thesis is made possible through the help and support of him. Thank you very much for giving me this wonderful opportunity. Under your guidance and encouragement I successfully surpassed many difficulties and learned a lot. You have given enough freedom during my research to encourage me becoming an independent thinker. You are a great advisor.

Second, I would like to express my thanks to Adama Science and Technology University for providing the necessary knowledge, assistance, facilities and financial support to conduct my research work, the Program of Applied physics, the Program of Material and science engineering for allowing me to use XRD, and the Program of Applied Biology for allowing me to use UV-Vis spectroscopy and SEM.

Third, I would like extend my thanks to my families who exhaustly helping me until now and supporting me by financial as well as encouraging me in every day to day.

Finally, I would like to thank all my friends who support me for their efficient coordination of the process of writing this thesis.

Dedication

Thesis dedicated to my father and mother whose love and encouragement never stop to sustain me!

Table of Contents

List of Tables

List of Figures

List of Acronyms and Abbreviations

B.subtillis	Bacillus subtilis
C.albicans	Candida albicans
E.coli	Escherichia coli
FWHM	Full width at half-maximum
NPS	Nanoparticles
NZ	No Zone
P.aeruginosa	Pseudomonas aeruginosa
ROS	Reactive oxygen species
S.aureus	Staphylococcus aureus
RE	Rare Earth
SEM	Scanning Electron Microscopy
TM	Transition Metal
UV-Vis	ultra violet -visible
XRD	x-ray diffraction
ZNO	zinc oxide
ZOI	Zone of inhibition

Abstract

In this thesis, ZnO nanoparticles were doped by Manganese (Mn) and Gadolium (Gd) successfully using chemical co-precipitation method. The effects of Mn and Gd dopants on the structural, morphological and optical properties of ZnO were investigated. In addition, the antimicrobial activity of ZnO nanoparticle doped by Mn and Gd metals was obtained. The structural, morphological and optical properties of these nanoparticles were characterized using X-ray diffraction (XRD), scanning electron microscope (SEM) and Ultra Violet-Visible (UV-Vis) spectroscopy. The *XRD results indicated all synthesized pure ZnO, Mn and Gd nanoparticles were possessed hexagonal phase of wurtzite structure and have average crystallite size ranged from 38 nm to 31 nm respectively. The decrease in crystallite size, lattice parameters, unit volume and bond length was observed after the incorporation of Mn and Gd ions into the ZnO matrix. On another hand, the increments in strain and concentration of defects were observed after the Mn and Gd dopants. From scanning electron microscopy (SEM) image, the nanosized spherical shape particles with well-defined distributions were observed. The energy band gaps estimated from Ultraviolet-visible (UV-Vis) absorption spectra found to be 3.35 eV, 3.28 eV and 3.07 eV for undoped ZnO, Gd doped and Mn doped, respectively. The antimicrobial activity of undoped, Mn and Gd doped- ZnO nanoparticles were tested against gram-negative bacteria (E. coli and P. aeruginosa), gram-positive bacteria (S. aureus and B. subtilis) and fungus (C. albicans) using agar-well diffusion method. The results indicated that the antimicrobial activity of doped ZnO nanoparticle increased as compared to undoped ZnO nanoparticle. It was also found that the gram-positive bacteria were more susceptible to ZnO nanoparticle than gram-negative bacteria and fungus.*

Keywords: Manganese-doped ZnO-NPs, Gadolium-doped ZnO nanoparticles, co-precipitation method, agar well diffusion method, E. coli, P. aeruginosa, S. aureus, B. subtilis and C. albicans

1. Introduction

1.1 Background of the study

Nanoparticles (NPs) are special class of organic or inorganic materials having size in the range of 1 to 100 nm in at least one dimension. NPs have unique and enhanced functional properties such as high surface area to volume ratio and more atoms on their surface than their micro-or macro-scale counterparts owing to their nanoscale feature [1]. Nanomaterials and nanotechnologies attract tremendous attention in recent research. Nanotechnology involves the manipulation of matter at nanometer scales to produce new materials, structures, and devices. Nanoparticles and nanotechnology are widely used in various biotechnological, pharmacological and technological uses [2].

Various synthesis approaches have been developed for synthesizing nanoparticles over the past few decades. Irrespective of the technique, the goal of particle synthesis generally focuses on: minimizing and controlling particle size, maintaining a narrow size distribution, control of particle morphology, and control of crystallinity. The ability to control size enables the variation of particle properties, while the narrow size distribution allows greater precision and is required for studies of size-dependent effects. Nanoparticles synthesis techniques can generally be divided into two classes: gas-phase methods and condensed phase methods. These two classes of nanoparticles synthesis are characterized by unique advantages and limitations. Out of many synthesizing techniques co-precipitation is good for the production of huge amount and high quality of nanoparticles at low cost rate and it requires low cost equipment. Within the co-precipitation synthesis technique, the particle size can be controlled by adjusting the pH value using inorganic base, the temperature of the reaction, the annealing temperature, and time [3].

Metal oxide nanoparticles are important materials, finding applications in a diverse range of activities. Among metal oxide NPs, ZnO NPs have many significant features such as chemical and physical stability, large exciton binding energy (60 mev), wide band gap, biosafe, biocompatibility, high catalytic activity, intensive ultraviolet (UV) and infrared (IR) adsorption. ZnO NPs also have several advantages due to low toxicity, biocompatibility and

biodegradability, which make the material important for anti-bacterial, anti-fungal, and wound healing applications [4].

Several studies have been conducted on various factors affecting the shape, size, optical properties and applications of ZnO NPs. The factors are precursor concentrations, temperature, surfactant concentrations, dopant concentrations, solvent medium and pH of the reaction mixture [1]. Doping is one of the strategies to modify the structural, morphological and optical properties of ZnO nanoparticles and enhance its applications such as antimicrobial activity. Doping ZnO with trace amounts of transition and rare earth metal ions has signicant changes in the optical, morphological and structural properties of ZnO NPs. Several reports are available regarding the doping of ZnO with metal ions (transition and rare earth elements) of Ni, Co, Fe, Mn, Cr, Al, Ag, Eu and Gd to change its properties for photocatalysis, sensors, and antimicrobial activity. Among the above dopants, Mn^{2+} and Gd^{3+} are favorable to incorporate into the ZnO lattice due to their same valence state (+2) and (+3) and similar ionic radii (Mn^{2+}, 0.66 A^o; Zn^{2+}, 0.74 A^o and Gd^{3+}, 1.95 A^o) [5-7].

The unique and new properties of nanomaterials have attracted scientists and researchers to the antimicrobial application. The research interest for the use of nanotechnology in the antimicrobial application has increased rapidly. Recently, microorganism pathogens have been a major problem to human health as well as to the environment. The nanotechnological applications in the field of biology have produced a completely new field of technology that is set to bring dramatic advances in the fight against various diseases. In this regard, many scientists and researchers are developing material with better antimicrobial and photocatalytic activity. Even though, there are the great progress in development of antimicrobial there are difficulty to treat many infectious diseases like intracellular infections. The reasons of difficulty are transportation through cell membranes, low activity in the cells, antimicrobial toxicity to healthy tissues and acquired resistance of infectious microbes. However, in nowadays nanosized materials have been emerged up as novel antimicrobial agents. Nanoparticles (NPs) exhibit better antimicrobial activity due to their large surface to volume ratio and high chemical reactivity or photocatalytic in comparison to bulk form. Many NPs have antimicrobial properties and used to control drug-resistant microbial populations. Various inorganic metal

oxide NPs such as ZnO, MgO, TiO_2 and SiO_2 show reasonably antimicrobial activities and used in therapeutics, diagnostics and nano medicine-based antimicrobial agents. Among inorganic NPs, ZnO nanoparticles show greater effectiveness on resistant strains of microbial pathogens, less toxicity, selectivity, better durability, heat resistance and provide mineral elements essential to human cells. Furthermore, there are several reports that deal with the particle size-dependent antimicrobial activity of ZnO nanoparticles (NPs), where antimicrobial activity is inversely related to the particle size. Hence, the crystal size of ZnO nanoparticles needs to be reduced for better antimicrobial activity. Accordingly, ZnO doped with Manganese and Gadolium has better antimicrobial activity as the dopants decrease the crystal size of ZnO nanoparticles [8-9].

The antimicrobial activity of undoped and doped zinc oxide nanoparticles has also been studied against gram-negative and gram-positive bacteria using chemically synthesizing method. The main mechanism of antimicrobial activities of ZnO NPs is the electrostatic interaction between ZnO NPs and cell membrane of the bacteria, penetration of ZnO NPs into the inside of bacterial cell wall, and the formation of reactive oxygen species (ROS) inside the cell of bacteria, which destroys the cytoplasm of the bacteria. It is reported that gram-negative bacteria are more resistant against ZnO NPs than gram-positive bacteria due to that it has double cell membrane structure (outside and cytoplasmic membrane) and the difference in intracellular antioxidant content [1].

1.2 Statement of the problem

Many researchers reported the synthesis and characterization of zinc oxide nanoparticle doped by Manganese (Mn) and Gadolium (Gd) metals in separate studies for different precursors at different conditions using different synthesis methods. But, to date results there is a controversial and debate on the influence of these dopants on the structural, morphological and optical properties as well as on the antimicrobial activity of ZnO nanoparticles. Therefore, in this research, it is intended to investigate the effects of Mn and Gd dopant ions on the structural, morphological and optical properties of ZnO nanoparticle and on its antimicrobial activity.

1.3 Objective of the study

1.3.1 General Objective

The general objective of this research work is to synthesize ZnO nanoparticles doped by Manganese (Mn) and Gadolium (Gd) using co-precipitation method and characterize their structural, morphological and optical properties for antimicrobial application.

1.3.2 Specific Objectives

The specific objectives are:

1. Synthesizing undoped and Mn and Gd doped zinc oxide nanoparticles using co-precipitation method.
2. Determining the structural, morphological and optical properties of pure and doped ZnO nanoparticles using XRD, SEM and Uv-Vis.
3. Analyzing the effect of Mn and Gd doping on the structural, morphological and optical properties of ZnO nanoparticles.
4. Comparing the antimicrobial activity of undoped and Mn and Gd doped ZnO nanoparticles.

The thesis is organized as follows. In Chapter 1, introduction to nanoparticles and nanotechnology, synthesis routes, factors affecting the structural, morphological and optical properties of ZnO nanoparticles, doped ZnO nanoparticles and its antimicrobial activity nanoparticles are presented. Statement of the problem and objective of the study are also presented in this chapter.

In Chapter 2, the crystal structure of ZnO nanoparticles, electronic properties, chemical properties and synthesis routes of ZnO NPs are presented in this chapter. Also transition metal and rare earth metal doped ZnO nanoparticles, applications of ZnO NPs, the characterization instruments used to characterize ZnO NPs crystal size, strain, dislocation density, volume of the unit cell, absorption peak and morphology are presented.

In Chapter 3, the materials and methods used in this work are presented. This chapter has five sections; the first section describes the chemicals and solvents used to carry out this research. The second section of this chapter deals with the apparatus and instruments used to

carry out this research. The third section describes the methods of synthesizing pure, Mn and Gd-doped zinc oxide nanoparticles from zinc, Manganese and Gadolium salt precursors. The fourth and fifth sections describe the antimicrobial activity and characterization mechanisms of undoped, Mn and Gd-doped ZnO NPs.

In Chapter 4, the results and discussion of the thesis are presented. The calculated values of crystal size, lattice parameters, unit cell volume, dislocation density and strain as well as absorption peaks (calculated band gap), morphologies and antimicrobial activities of undoped, Mn and Gd-doped ZnO NPs are presented. Finally, the thesis is ended up with the conclusion in Chapter 5.

2. Literature Review

In this Chapter, the literature review related to nanotechnology and nanomaterial, the crystal structure of ZnO nanoparticles, electronic properties, chemical properties and synthesis routes of ZnO NPs are presented. And also the zinc oxide nanoparticles doped by transition and rare earth metals, the characterization techniques and applications of ZnO NPs are reviewed.

2.1 Nanomaterials

Nanoparticles are particles that exist on a nanometer scale below 100 nm at least in one dimension. They can possess unique chemical and physical properties such as uniformity, conductance or special optical properties that make them desirable in different area of research and applications in various fields such as electronics, optical communications and biological systems. Recently, materials at nanoscale are attracting the interest of many researchers and scientists because materials at this level exhibit special optical, electrical and magnetic properties which are significantly different from those at a larger scale [1].

Nanomaterials can be produced in different shapes (spherical, rod, tube and wire) based on different synthesizing parameters such as temperature, solvents, precursors, reaction time and pressure. These materials can exist in different dimensions; in one dimension (nanowires and nanotubes), in two dimensions (very thin surface coatings) or in all three dimensions (nanoflowers). As a particle decreases in size, a greater proportion of atoms are found at the surface compared to those inside. Thus nanoparticles have a much greater surface area per unit mass or high surface area to volume ratio compared with larger particles. Nanoparticles have high chemical reactivity or chemical catalytic activity than the same mass of material made up of larger particles due to the fact that the growth and catalytic chemical reactions occur at surfaces [10].

2.2 Nanoscience and Nanotechnology

Nanoscience is the study of phenomena and manipulation of materials at atomic, molecular and micro molecular levels, where properties differ significantly from those at a larger scale where as nanotechnology is the design, creation, characterization, exploitation and utilization of structures,

devices and systems by controlling shape and size at the nanometer scale. In order words, nanotechnology is deal with the engineering of functional systems and applications of nanoscale materials that have size and structural features lay between those of atoms and their bulk materials, new properties and functions. Nanotechnology has been subject to various discussions and developments during last six decades, starting from Richard Feynman's speech, "There's Plenty of Room at the Bottom" in the annual meeting of the American physical society at California Institute of Technology on 26 December 1959 and followed by the introduction of the word "Nanotechnology" in 1974 by Norio Taniguchi. Richard Feynman, in his this famous lecture he suggested that it would be possible to arrange the atoms the way we want and synthesize any chemical substance by putting atoms down as we desire. [11].

2.3 ZnO Properties

2.3.1 Crystal structure of ZnO

Zinc oxide (ZnO) is an inexpensive material and is relatively abundant. It has high chemical and thermal stability, high electrochemical coupling coefficient, broad range of absorption radiation, high photostability with multifunctional material and non-toxic, easy to prepare and therefore, it is one of the widely investigated materials. It has many useful properties such as high carrier mobility, large exciton-binding energy (60 meV), low toxicity, biocompatibility, biodegradability, transparency and a wide band gap of 3.37 eV. ZnO occurs in nature as the mineral zincite. ZnO can possess 4 crystal structures: cubic zincblende, rocksalt, cubic caesium chloride, and wurtzite (B4 type) structure. Among them, wurtzite structure is the most common stable ZnO phase at ambient pressure and temperature. This structure is related to a hexagonal close packed (HCP) structure with zinc atoms and oxygen atoms tetrahedral four-coordinated as shown in Figure 2.1 below. Wurtzite zinc oxide has a hexagonal structure which belong to space group C6mc and it has lattice parameters a = 0.3296 nm and c = 0.52065 nm, in the ratio of 1.611. The structure of ZnO contains a number of alternating planes composed of tetrahedrally coordinated $O^{2-}$and Zn^{2+} ions, stacked alternately along the c-axis (Figure 2.1). The tetrahedral coordination in ZnO results in noncentral symmetric structure which consequently gives piezoelectricity and pyroelectricity. Another important characteristic of ZnO is polar surfaces. The most common polar surface is the basal plane. The oppositely charged ions produce positively charged Zn-(0001) and negatively charged O-(000$\bar{1}$) surfaces, resulting in a normal

dipole moment and spontaneous polarization along the c-axis as well as a divergence in surface energy [15].

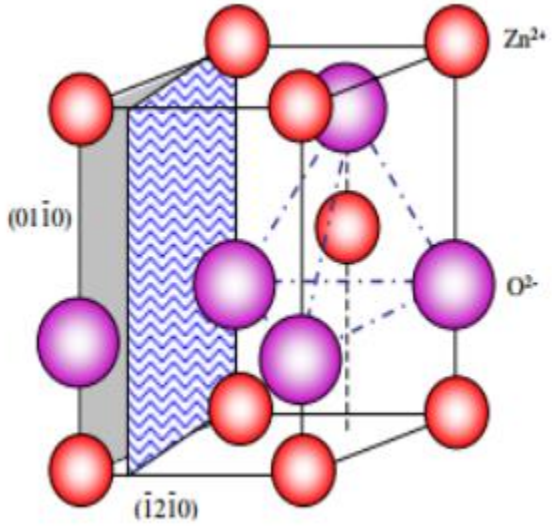

Figure 2.1: The wurtzite structure model of ZnO [16]

Since ZnO wurtzite is known to be a Hexagonal system, the lattice parameter a and c for crystallographic systems in the present study can be calculated from the following equation using the (hkl) parameters and the interplanar d spacing as follows.

$$d = \frac{1}{\sqrt{\frac{4}{3}\left(\frac{h^2 + hk + k^2}{a^2}\right) + \frac{l^2}{c^2}}} \qquad (2.1)$$

Where 'a' and 'c' are the lattice constants and h, k, l are the Miller indices along a, b, and c-axis respectively [8].

2.3.2 Basic physical parameter for Wurtzite ZnO

The fundamental properties of the nanomaterials are indispensable for nanotechnology applications. So, one must know and understand the fundamental physical properties of ZnO for the rational design of functional and new materials. It is obvious that as the dimension of the semiconductor materials approach to nanometer scale, some of their physical properties undergo changes due to "quantum confinement size effects". Table 2.1 shows some of the basic physical parameters for wurtzite ZnO [17-20].

Table 2.1 Some fundamental physical parameters of wurtzite ZnO.

Physical parameter		Values
Lattice parameters at 300 K	a_0	0.324 95 nm
	c_0	0.520 69 nm
	a_0/c_0	1.602 (ideal hexagonal structure 1.633)
	U	0.345
Density		$5.606\ g/cm^3$
Stable phase at 300 K		Wurtzite
Melting point		2248 K
Linear expansion coefficient ($/^oC$)		a_0: 6.5×10^{-6}
		c_0:3.9×10^{-6}
Static dielectric constant		8.656
Refractive index		2.008, 2.029
Energy gap (300 K)		3.37 eV (direct band gap)
Intrinsic carrier concentration		$<10^6\ cm^{-3}$ (max n-type doping$>10^{20}cm^3$ electrons; max p-type doping$<10^{17}cm^{-3}$ holes)
Exciton binding energy		60 meV
Ionicity		62%

Electron effective mass	0.24
Electron mobility (T = 300 K)	200 $cm^2/V.s$
Hole effective mass	0.59
Hole mobility (T = 300 K)	5-50 $cm^2/V.s$

2.3.3 Chemical properties of ZnO

Naturally, ZnO appears as a white powder known as mineral zincite or zinc white. It usually contains some manganese particles or other impurities that change its colour from white to red or yellow [21]. Upon heating zinc oxide always alters its color from white to yellow owing to the loss of oxygen (deficiency of oxygen). Again when cooled down it turns back into its original color by regaining oxygen. ZnO is an amphoteric semiconductor oxide that is insoluble in water and alcohol, but soluble in degrading acids such as hydrochloric acid (HCl):

$$ZnO + 2HCl \rightarrow ZnCl_2 + H_2O$$

When reacted with phosphoric acid, it forms cement-like zinc phosphate cements. Since ZnO is in powder form bases can also degrade it into soluble zincates:

$$ZnO + 2NaOH + H_2O \rightarrow Na_2 (Zn (OH)_4)$$ [22-24].

2.3.4 Optical properties

The optical properties of nanomaterials depend strongly on their dimensions and surface Plasmon resonance. The effect of dimension on the optical properties of nanomaterials can be explained as follows. As the size of nanomaterials is decreased (quantum confinement size effect), the number of atoms in the material will be decreased. This reduction in the number of atoms in a material results in the confinement of normally delocalized energy states and electron-hole pairs or free exciton. As a result the spacing between the energy bands of a semiconductor is increased and its absorbance as well as luminescence shifts to blue. Thus, optical properties of such materials are easily tailored by varying particle size. Generally, the optical properties of a semiconductor are related to its intrinsic and extrinsic factors. Intrinsic optical properties related to the relation between electrons in the conduction band (CB) and holes in the valence band (VB) or band to band transition and also including excitonic effects due to the Coulomb interaction.

Extrinsic properties are related to dopants (impurities) or defects produced in the semiconductor, which introduce new discrete electronic states in the forbidden band gap. Various experimental techniques such as optical absorption are widely used to investigate the optical property of ZnO. A. B. Djurisic et. found that the Optical properties of ZnO nanostructures highly affected by dopants and impurities. [25-28].

2.4 Characteristics of Transition Metal (TM)-doped ZnO and Characteristics of Rare Earth (RE)-doped ZnO

The structural, electrical, optical and magnetic properties of ZnO properties and also the efficiency of its function can be substantially modified by various doping elements to the ZnO crystals. Dilute magnetic properties of transition metal doped semiconductors, called diluted magnetic semiconductors (DMS), provide an alternative way to make the semiconductors ferromagnetic at room temperature. For example, by doping transition magnetic elements such as Co, Mn, Fe and Ni in to ZnO lattice we can tailor it for optoelectronic, spintronics and high performance sensors based devices as well as its photocatalytic and antimicrobial activity can be enhanced. The synthesis of ferromagnetic semiconductors that works at room temperature remains very attractive for device applications such as emitter and detector. The 3d TM ions fundamental properties of ZnO and TM-doped ZnO such as Sc, Ti, V, Cr, Mn, Fe, Co, Ni, and Cu have partially filled d shells are substituted for the cations of the host semiconductors, which leads to achieve the DMS. These elements are easily incorporated into ZnO host lattice as they have ionic radii close to Zn and they are useful due to their high electrical conductivity. The magnetic property of a DMS is found to be a strong function of the TM ions concentration in the crystal, the carrier density, and the crystal quality [29]. For doping of ZnO, rare earth elements are more likely to be considered as dopants due to their characteristic luminescence and high conductivity properties [30]. ZnO doped with rare earth metals provide wide bandgap semiconductors and are very useful for displaying different applications such as UV, visible, and infrared light emission. Wide band gap exhibits less thermal quenching of emissions than narrow gap semi-conductors. Gd doped ZnO materials have been effective due to its scintillation properties, UV optical characteristics, photocatalytic activity, antibacterial and antifungal activity as well as room temperature ferromagnetism. X. H. Zhang et al. fabricated high sensibility gas sensors based on Erbium doped and Gadolium ZnO nanocrystals and found green luminescence

from Eu-doped ZnO and red luminescence from Gd-doped ZnO suggesting that these materials may prove useful in optoelectronic applications [31].

2.5 Synthesis routes of zinc oxide nanoparticles

Several synthetic approaches have been developed for synthesizing zinc oxide nanoparticles over the past several decades. Regardless of the technique, the goal of particle synthesis generally focuses on: minimizing and controlling particle size, maintaining a narrow size distribution, control of particle morphology, and control of crystallinity. The ability to control size enables the variation of particle properties, while the narrow size distribution allows greater precision and is required for studies of size-dependent effects. Particle shape and crystal structure can also influence material properties. Nanoparticle synthesis techniques can generally be divided into two classes: bottom up and top down approaches [32].

Bottom up approach technique individual atoms and molecules are brought together or self-assembled to form nanostructured materials at least in one dimension. All the techniques that start with liquid and gas as the starting material fall into this category. Usually, this technique can give very fine nanostructures of individual nanoparticles, nanoshells, etc., with narrow size distributions, if the process parameters are effectively controlled. On another hand, in Top down approach technique a macro crystalline material is fragmented to yield a nanocrystalline material. All the solid state routes fall into this category. This technique does not usually lead to individual nanoparticles; however, they produce bulk nanostructured materials [32].

2.5.1 Co-Precipitation Method

Co-precipitation involves a stoichiometric mixture of soluble salts of metal and precipitating them as hydroxides, oxalates, citrates or formats. It takes place when any solution is supersaturated to form precipitates with another substance. In this method, an inorganic metal salt is dissolved in solvent and these formed species are hydrolyzed by adding a basic solution example NaOH or KOH. By the action of cationic solution, solutions are condensed with each other to form a metal hydroxide precipitate. The formed precipitate has undergone several processes, such as filtration, annealing and drying to collect nanopowders of crystalline metal oxides. Co-precipitation technique provides nanopowders with good quality despite of the low cost and simplicity of this method [33].

Another useful method is sol-gel method. Sol–gel method is the process for obtaining crystalline materials from a very tiny molecule. This process involves a formation of an inorganic network of colloidal suspension (sol) followed by gelation of the sol solution to form a continuous liquid phase (gel). Thus formed gel can be used to fabricate various nanomaterials and nanostructures such as powders, aerogels, xerogels, etc. There are number of precursors that can serve as sol forming constitutes such as, metal alkoxides, metal organic compounds, salts of inorganic acids, salts of organic acids, etc. However, the most commonly used precursors are metal alkoxides; compounds in which a metal is bonded to one or more alkyl groups through an intermediate oxygen atom. Addition of acid or base catalyst is also common in sol-gel processes to increase the rate of the reaction. This method can be used for the fabrication purposes, mainly of metal oxides, such as silicon. In this process, the monomers are converted into colloidal solutions acting as precursors for the gel formation using discrete particles. The precursors that can serve the function of precursor materials, they will undergo hydrolysis of and polycondensation processes to form M-O-M bonds. In the hydrolysis process, as the name suggests, precursor will hydrolyze and attains a hydroxyl group typically through the reaction with water. Polycondensation is the process in which hydrolyzed species combine to make a inorganic polymer like chains through elimination of a water molecule. Finally, with filteration and drying process the desired nanostructures that have will be synthesized [33].

Several different methods also exist for obtaining nanoparticles of different sizes and shapes. Those are paralysis spray method, sonochemical method, combustion method, thermal evaporation, microwave assisted, and electro spinning method, etc [33].

2.6 Application of ZnO NPs

The unique structural, mechanical, electrical and optical properties of nanoparticles are dependent of the surface Plasmon resonance and quantum size confinement. ZnO NPs are widely used in many applications as NEMS systems, single electron transistors, engineered solar cells, OLED's, laser diodes and many other optoelectronic devices due to special properties [34, 35]. In addition, due to their unique and versatile features and properties, the transition metals-doped ZnO nanoparticles can be used in various industrial applications. The TM-doped and RE-doped ZnO nanoparticles have major applications in various fields compared with

undoped ZnO nanparticles. They are used in the field of electronics and semiconductor industry for developing single electron transistors, photodetectors, fabricated LEDs, laser diodes, flat panel displays, transparent electrodes, nanogenerators, solar cells, optical waveguides, PZT transducers, surface acoustic wave devices, water treatment, optoelectronic devices, etc. They are used in the field of spintronics for making solid state devices for memory storage and electro-magnetic devices. They are used in sensing applications and for biomedical applications including antimicrobial activity [36].

In recent time, a lot of serious human health and environmental issues were caused by the increasing resistance of pathogen agents towards antibiotics. Researches could reveal novel application of metals as intrinsic antimicrobial activity by combining advanced technologies of material science and material engineering respectively [37]. Numbers of metals and compounds of nanomaterials have been used as antimicrobial agents to control pathogenic microorganisms. Nanoscaled metals and inorganic compounds have shown remarkable antibacterial activity even at very low concentration due to their high surface area to volume ratio and unique chemical and physical features. In addition, these particles are biocompatible, biosafe, nontoxic and also more stable at high temperature and pressure. In general, zinc oxide nanomaterials exhibited important biological activities and structural properties. Bacterial and fungal population is naturally capable of developing resistance against antibiotics and metals and spreads more potential and creates health problems, drug resistance in bacteria and fungal leading to ineffectiveness of medicine for treatment of a number of diseases [38].

The main mechanism of antimicrobial activities of ZnO NPs is the electrostatic interaction between ZnO NPs and cell wall of the bacteria, internalizations of ZnO NPs into the cell of bacteria, and the generation of reactive oxygen species (ROS) inside the cell of bacteria, which destroys the cell wall, the cytoplasm and all intracellular components of the bacteria [1]. The ROS production mechanisms driven by ZnO NPs are described in Figure 2.2.

Since ZnO is a semiconductor, it’s the electronic band structure has a conduction band (CB) and a valence band (VB). When photon radiation (hv) of energy greater than the bandgap of ZnO (higher than 3.3 eV) interacts with ZnO, it is immediately absorbed and electrons will move from the VB to the CB, which initiates a series of photoreactions. Following this step,

Positive holes (h^+) are created in the VB and, in turn, there are free electrons (e−) in the CB. These electron pairs (free exciton) initiate various reactions. The "holes" separate water molecules into OH^- and H^+. The free electron pair of the CB reacts with the dissolved oxygen molecules and it transforms into superoxide radical anions (O_2−), which react with H^+ and give (HO_2) radicals that after colliding with the electrons are transformed into hydroxyl peroxide anions (HO_2−). These, in turn, can react with hydrogen ions and produce hydrogen peroxide (H_2O_2) that can penetrate into bacterial cell wall and kill microorganisms [39].

The release of Zn^{2+} ions is also another way to destroy or kill bacteria. When ZnO NPs are in solution, partial dissolution results in the release of Zn^{2+} ions, which have antimicrobial activity. This dissolution of ZnO NPs decreases the amino acid metabolism and perturbs the enzymatic system which contributes to its antimicrobial activity. In Addition, to improve the ZnO photocatalytic properties and antimicrobial activity it can be doped with transition metals (Mn, Cu, Co) and rare earth metals (Eu, Gd) as they results in changes to the surface area due to the introduction of dopant ions. Thus, the presence of impurities in semiconductor NPs can lead to significant changes in their structural, electrical and optical properties. The incorporation of dopants during the nanostructure formation process will results in new crystal growth conditions, morphology and creating many defects such as oxygen vacancy, oxygen interstitial, zinc vacancy and zinc interstitial in their structure. These defects, specially enhanced oxygen vacancy favours photocatalytic reactions, and therefore a higher amount of ROS is generated. Hence, higher ROS concentrations result in greater antimicrobial activity by ZnO NPs as ROS generation is a major mechanism responsible for ZnO NPs antimicrobial activity. In addition, the presence of dopant ions in ZnO NPs has been used in some studies to assess their relationships with the antimicrobial activity of ZnO NPs. The presence of these dopant ions can significantly alter the size of ZnO NPs (they decrease their size). This enhances the antimicrobial effect of NPs due to the decrement in size results in large surface area and higher chemical reactivity [37-39].

Various researchers have tried to dope transition and rare earth metal dopants into the ZnO lattice, to enhance the antibacterial activity of ZnO. For example, K. Rekha et al. synthesized Mn doped ZnO for antibacterial activity of ZnO. Similarly, Manjulaet al.synthesized Co doped ZnO and did its antibacterial activity using disc diffusion method, which was found to

be enhanced after Co doping. Bomila et doped Cu into the ZnO lattice to enhance its antibacterial activity. They reported that the doping of Cu increased the antibacterial activity against Escherichia coli, Staphylococcus aureus bacterial and Candida albicans yeast pathogens. All these studies confirm that the doping of transition metal ions and rare earth ions increase the antibacterial as well as the antifungal activity of the ZnO. Yet, these doping were found to decrease the crystallinity of the ZnO, which could reduce its stability, during in-vivo applications [39]. The previous literature indicated gram-positive bacteria have higher susceptibility to ZnO NPs than gram-negative bacteria due to that they have simpler or single cell membrane structure and the difference in their chemical composition as well as intracellular antioxidant content [1].

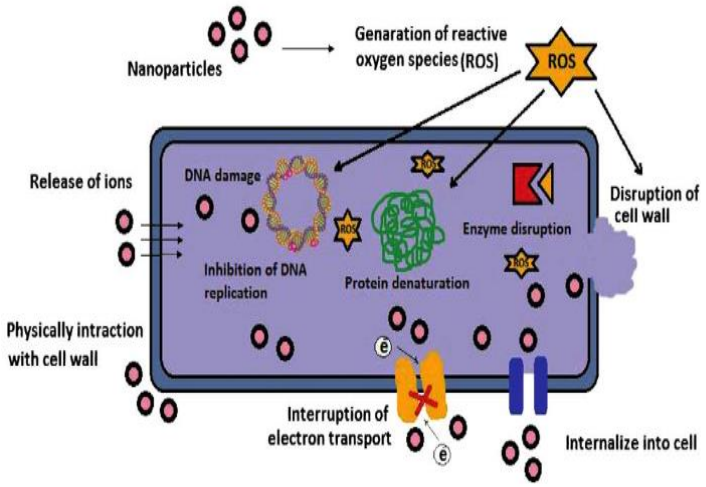

Figure 2.2: Various mechanisms of antimicrobial activity of the metal nanoparticles [37].

2.7 Characterization of ZnO NPs

2.7.1 X-ray diffraction (XRD)

X-rays were discovered by Wilhelm Rontgen, a German scientist in 1895 and before that it was very difficult to investigate materials at angstron level. The powder XRD is the most common and first hand instrument used by solid-state scientists. A great advantage of X-ray powder diffraction is that it requires no sample preparation in contrast to other techniques. The sample can be either in the form of smear or compact flat pack or a capillary. X- ray diffraction is a powerful method to investigate cystalline solids. Crystalline solids consist of regular arrays of

atoms, ion, or molecules with interatomic spacing on the order of 10^{-10}m. The wavelength of the incident light has to be on the same order as the spacing of the atoms. Source of electrons (cathode) and anode are very essential for generating this X-rays. Source of electrons (cathode) is used for accelerating the electrons at high speeds and anode for receiving the impact of the electrons and interact with them. A typical cathode element is Tungsten (W) with potential of 20-50 KV and the anodic material should be water cooled. The frequency (wavelength) depends on the anode material, usually Cu, Mo, or Co. Different lines occur when electrons knock out the target material and remove electrons from K shell ($n = 1$), which are filled by electrons in higher shells. Electrons falling from L shell ($n = 2$) give rise to lines $K_{\alpha,}$ whereas from M($n = 3$) shell give the K_{b} lines. The characteristics K_{α} x-ray is needed and selected. However, line K_{β} is filtered out by using a thin metal foil of the adjacent element ($Z - 1$), for example Nickel filters line of copper. A monochromatic beam of X-rays can also be selected by reflecting from a plane of a single crystal [40].

During the analysis of XRD measurement, X-Rays strike the sample specimen and the electron clouds of atoms in the sample are scattered elastically. Detector is then used to measure the X-Ray intensity as a function of the angle of beam diffraction. A periodic structure within the sample leads to interference fringes determined by the periodic arrangement of the atoms. The intensity corresponding to a constructive interference of the diffracted beam from a crystallographic plane is observed as peak, corresponding to the Bragg angle (θ). Thus Bragg's Law Eq (2.2) plays a crucial role in interpretation of these peaks.

$$\lambda = 2d\sin\theta \tag{2.2}$$

Where d is the distance between the atomic planes, θ being the scattering angle, and λ being the wavelength of the incident X-ray radiation. By making the use of the Bragg law of Eq. (2.2), the lattice parameter 'a' is calculated for (1 0 0) plane using following Eq. (2.3).

$$a = \frac{1}{\sqrt{3}}\frac{\lambda}{\sin\theta} \tag{2.3}$$

For the plane (0 0 2) the lattice parameter c is calculated using the following Eq. (2.4).

$$c = \frac{\lambda}{\sin\theta} \tag{2.4}$$

The dislocation densities (δ) of ZnO NPs are calculated by the Eq. (2. 5).

$$\delta = \frac{1}{D^2} \tag{2.5}$$

Where D is the crystalline size.

The micro-strain (ε) is estimated from:

$$\varepsilon = \frac{\beta\cos\theta}{4} \tag{2.6}$$

The volume (V) of the unit cell of ZnO is given by Eq. (2.7).

$$V = 0.866a^2c \tag{2.7}$$

The bond lengths (L) and the positional parameter (u) are given by

$$L = \sqrt{\left(\frac{a^2}{3} + \left(\frac{1}{2} - u\right)^2 c^2\right)} \tag{2.8}$$

$$u = \frac{a^2}{3c^2} + 0.25 \tag{2.9}$$

G. Vijayaprasath et al. synthesized Ni/Mn co-doped ZnO nanoparticles by co-precipitation method and found lattice parameters a= 3.25 A^o and c= 5.206 A^o, bond length and positional parameter with the values of 1.979 A^o and 0.379 A^o ,respectively

A XRD powder diffraction patterns provide information about phases, peak positions, phase height, structure, degree of crystallinity or amorphous content, lattice parameters, interplanar spacing, volume of the unit cell, strain, dislocation density, crystallite size or peak widths/broadening. The most intense and well-defined peaks show strong reflections (diffraction) from various crystal planes. The positions of the peaks provide an accurate fingerprint of the crystal structure of the nanocrystals. The width of the peaks in a particular phase is an indicator

of the average crystallite size. Large crystallites give rise to sharp peaks, while the peak width increases as crystallite size reduces [41].

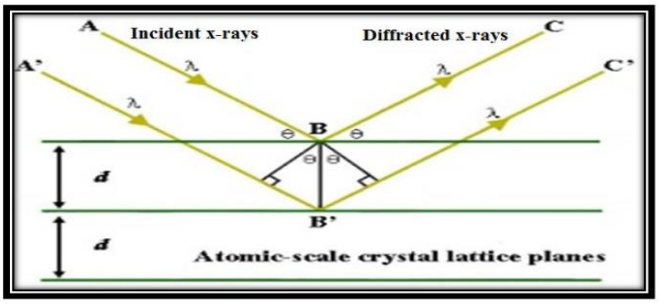

Figure 2.3: Bragg's law of diffraction [41].

In addition to determining crystal phase, the line widths can be used to estimate the mean crystal size of a sample by use of the Scherrer's Eq. (2.10) [42].

$$D = \frac{k\lambda}{\beta \cos\theta} \tag{2.10}$$

Where D is the mean size of the crystalline domains, which may be smaller or equal to the grain size; K is a dimensionless shape factor, with a value close to unity. The shape factor has a typical value of about 0.89, but varies with the actual shape of the crystallite. λ is the X-ray wavelength, which depends on the X-ray sources. β is the line broadening full width at half the maximum intensity (FWHM) in radians, θ is the Bragg angle [43].

2.7.2 Scanning Electron Microscopy (SEM)

Scanning electron microscopy (SEM) is a technique that uses highly focused beam of high-energy electrons (eV-150 eV) that interacts with a sample to produce various signals (secondary electrons, reflected or back scattered electrons, characteristics x-rays and transmitted electrons) that contain information about topography, morphology and crystallography of the sample [44]. In secondary electron imaging (SEI), the secondary electrons are emitted inelastically from very close to the specimen surface. These secondary electrons have less energy than incident electrons. Consequently, SEI can produce very high-resolution images of a sample surface, showing details less than 1 nm in size and it gives information about the morphology of the surface. Back-scattered electrons (BSE) are beam electrons that are reflected from the sample by

elastic scattering. They emerge from deeper locations within the specimen and, consequently, the resolution of BSE images is less than SE images. However, BSE are often used in analytical SEM, along with the spectra made from the characteristic X-rays, because the intensity of the BSE signal is strongly related to the atomic number (Z) of the specimen.

In a typical SEM, a beam passes through pairs of scanning coils or pairs of deflector plates in the electron column to final lenses, which deflect the beam horizontally or vertically. The image displayed is therefore a distribution map of intensity of signal being emitted from the scanned area of the specimen. Mostly data is collected over a selected area of the surface of the sample, and a 2-D image that displays spatial variations in these properties is generated [45].

The system can also provide qualitative chemical analysis if it is equipped with a dispersive X-ray spectrometer (EDS). In a typical SEM system, a beam of accelerated electrons with significant amounts of kinetic energy strikes the surface of the sample and generates a splash of electrons with kinetic energies much lower than primary incident electrons called secondary electrons (that produce SEM images). To create a SEM image, the secondary electron intensity is measured as a function of the primary beam position [46].

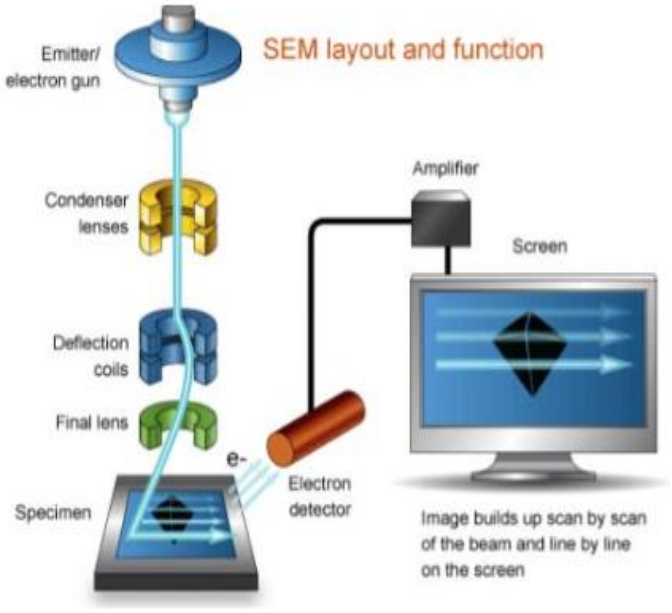

Figure 2.4: Operation of the SEM instrument [47].

2.7.3 Ultraviolet-visible spectroscopy

The UV-Vis Spectroscopy is the most important an analytical technique in the modern day laboratory. (UV-Vis) refers to absorption spectroscopy or reflectance spectroscopy in the ultraviolet-visible region. The UV-visible range covers some part of the total electromagnetic spectrum, and is generally ranges from wavelengths of 190 nm at the high energy UV end to about 750 nm at the low energy red end of the spectrum. The UV-visible spectroscopy is used to study molecules and inorganic ions in solution as well as in the solid state.

UV-vis spectroscopy technique deals with characterizing the intensity of light passing through a sample in the ultraviolet and visible regions in terms of wavelength expressed in nanometers. It is almost entirely used for quantitative analysis; that is, the estimation of the amount of a compound known to be present in the sample. Light of other regions of the spectrum gives rise to different types of transitions and hence different types of spectroscopy [48].

The processes concerned in absorption spectrometry are absorption and transmission based on the Lambert's Law which states that each layer of equal thickness of an absorbing medium absorbs an equal fraction of the radiant energy that traverses it. When light travels through a thin slice Δx of absorbing sample, its intensity diminishes by an amount proportional to the initial intensity Io and the thickness of the slice. According to beer-lamberts law the interaction of light with matter gives an exponential attenuation relating to the incoming light Io to the thickness Δx.

$$I(x+\Delta x) = I(x) - I(x)\alpha\Delta x \tag{2.11}$$

This can be rewritten in the form

$$\lim_{\Delta x \to 0} \frac{I(x+\Delta x) - I(x)}{\Delta x} = -\alpha I(x) = \frac{dI}{dX} \tag{2.12}$$

Eq. (2.12) is a differential equation with the solution

$$I(x) = I_o \exp[-\alpha x] \tag{2.13}$$

When ultraviolet or visible light strike atoms or molecules they can either bounce off or cause electron to jump between energy levels. Absorption of ultraviolet or visible light electromagnetic radiation causes electron to move from lower energy levels to higher energy levels. Above a certain energy or frequency known as the absorption edge, intense absorption occurs. Absorption of visible and ultraviolet (UV) radiation is associated with excitation of electrons in nanoparticles from lower to higher energy levels. Since the energy levels of matter are quantized, only light with the precise amount of energy can cause transitions from one level to another will be absorbed. An electron is excited from a ground state into an excited state. Each wavelength of light has a particular energy associated with it. If that particular amount of energy is just right for making one of these electronic transitions, then that wavelength will be absorbed. The wavelength that is absorbed depends on the chemical composition. The intensity of the band is directly proportional to the concentration of an absorbing group or molecule. The larger the gap between the energy levels, the greater the energy required to promote the electron to the higher energy level; resulting in light of higher frequency, and therefore shorter wavelength, being absorbed [49]. Nanoparticles undergo electronic excitation following absorption of light. Absorption of light in the UV-visible region will only result in the following transition.

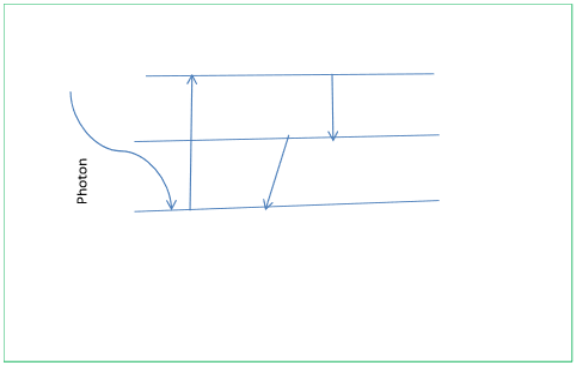

Figure 2.5: Absorption and Electronic transition of nanoparticles [50].

UV-visible spectrometers measures the intensity of light passing through a sample (I), and compares it to the intensity of light before it passes through the sample (Io). If the intensity of the incident radiation is Io and that of the transmitted light is I , then the fraction transmitted ($\frac{I}{Io}$) is called the transmittance (T) and is usually expressed as a percentage (%T).

The percentage transmission is

$$\%T = \frac{I}{Io} x100 \tag{2.14}$$

UV-visible spectroscopy enables the characterization of functional groups in a molecule as well as the determination of their concentration as per Beer-Lamberts law of Eq. (2.15).

$$A(\lambda) = -\log\frac{I}{Io} = \log\frac{Io}{I} = \varepsilon cL \tag{2.15}$$

Where $A(\lambda)$ is UV-Vis absorbance, Io is light entered to sample and I the light transmitted from the sample. The absorbance, A, is based on the transmittance [49, 50].

$$A = -\log\left(\frac{\%T}{100\%}\right) \tag{2.16}$$

The parameter that can be determined from the UV-vis spectra is the energy band gap of the samples. The band gap energies are calculated using the equation of the reference,

$$Eg = \frac{hc}{\lambda} = \frac{1240}{\lambda \max} \text{ eV} \tag{2.17}$$

Where h is the Planck's constant (6.626×10^{-34} Js), c is the light velocity (3×10^{8}m/s) and λmax is the wavelength in nanometer [51].

A schematic diagram of a UV-visible spectrometer is shown below.

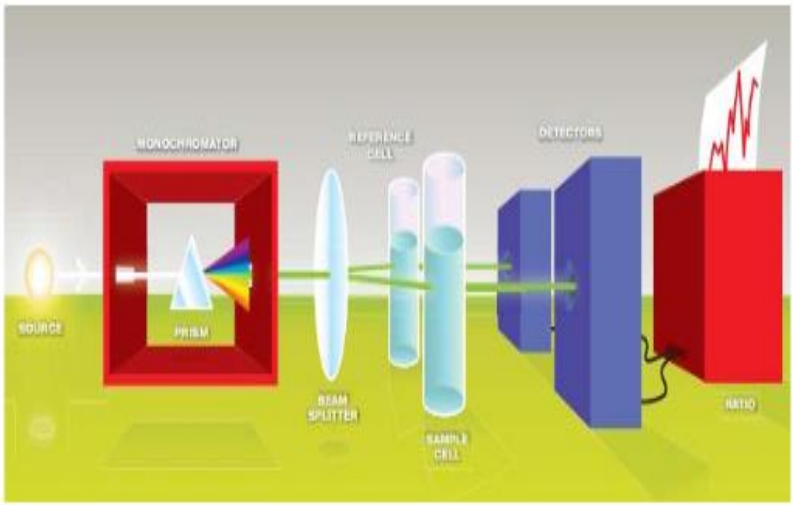

Figure 2.6: Operation of the UV-Vis instrument [51]

3. Materials and Methods

In this chapter, the materials and methods of the thesis are presented. The first section gives a detailed account of chemicals and solvents used to carry out this research work. The second section of this chapter deals with the apparatus used to carry out this research work. The third section describes methods of synthesizing undoped and (Mn, Gd) doped zinc oxide nanoparticles. The fourth and fifth sections describe the determination of antimicrobial activity and the characterization techniques of pure and doped ZnO nanoparticles.

3.1 Chemicals and Samples

Materials and chemicals used for the synthesis of pure and doped ZnO NPs were zinc acetate dihydrate (Zn $(CH_3COO)_2.2H_2O$) (UniChem, India), sodium hydroxide (Alpha Chemika, India), Manganese acetate dihydrate (Mn $(CH_3COO)_2.2H_2O$) (UniMagmedia, india) and Gadolium hexahydrate (Gd $(CH_3COO)_3.6H_2O$) (uniHimedia, India)**.** Culture media such as Müller-Hinton agar (MHA) (M173-500G HiMedia India), tryptone soya agar (TSA) (T131-500G HiMedia, India), and nutrient broth (N173-500G HiMedia India) for cultivation of the test organisms was used for the determination of antimicrobial activity of ZnO nanoparticles. Dimethyl sulfoxide (DMSO) (99% Unichem, India), Ethanol and double distilled water were used as the solvent. Antibiotic Gentamicin was used as positive control. All chemicals were of analytical grade with 99.9 percent and didn't undergo further purification.

3.2 Apparatus and instruments

Some of the laboratory apparatus used to synthesis pure and doped ZnO nanoparticles were cylinders, pipettes, magnetic stirrer (MH 2It.) (used to stir the mixture), beakers, filter paper (Watt Mann. 1) (used to separate precipitate from the mixture), spatula, Ceramic crucible cups (used to hold the stock solution in the furnace and as well as in the drying oven), analytic balance (FA.Model 2104) (used to measure the mass of sodium hydroxide, Zinc acetate dihydrate, Manganese acetate dihydrate and Gadolium acetate hexahydrate), oven (Model-DGH-9055, Jangasu Gangdu Mechanic Eectronic Equipment Co.Ltd.,China) (used to dry wet nanoparticles)

and furnace (Model-BK-5-12GJ, Biobase Biodustry Shangdong Co. Ltd., China) (used for annealing the powder). The apparatus used for culturing of bacterial and fungus were Petri plates (dish), Micro petite, Test tubes , Aluminum foil , Gloves, Sterilizer, Incubator, Cotton swab , Refrigerator(LG) and Ruler. And also the laboratory instruments used to characterize undoped and doped ZnO nanoparticles were scanning electron microscopy (SEM) to characterize nanoparticles morphology, UV-Vis spectroscopy used to study the optical properties (band gap) and X-ray powder used to characterize crystal structure as well as strain and dislocation density in crystal lattice. Some of the apparatus and equipment used are shown in Figure 3.1.

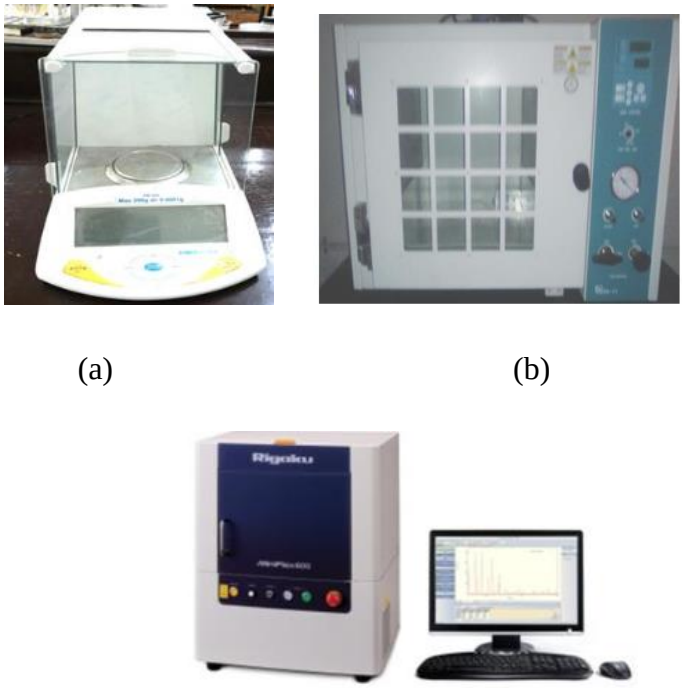

(a) (b)

(c)

Figure 3.1: Some of the apparatus and equipment used (a) Digital Balance (b) Vacuum Oven and (c) X-ray equipment

3.3 Methods of the experiment

First laboratory apparatus such as cylinders, pipettes, magnetic stirrer, beakers and spatula were cleaned and dried. Also, analytic balance, oven and furnace were calibrated properly. After that, undoped ZnO, $Zn_{0.98}Mn_{0.02}O$ and $Zn_{0.98}Gd_{0.02}O$ were synthesized using following procedures. In the synthesis of pure ZnO, 21.95 g of zinc acetate dihydrate was completely dissolved in 100 ml of deionized water and 0.2 M of aqueous NaOH solution (0.01 mol of NaOH dissolved in 50 ml

of deionized water) was added drop wise to the mixture. Later, the solution was stirred at room temperature for 30 min and then placed at room temperature (28 -30 ℃) for 5 hr for precipitation to occur. This resulted in the formation of white colored precipitates in the reaction mixture. To separate the precipitates, the reaction mixture was filtered and washed several times with double distilled water and ethanol to remove impurities. Thereafter, it was oven-dried at 60 ℃ for 17 hr. The dried precipitates were milled using a pestle and mortar, and then the powder was heated in oven for 20 min at the same temperature (60 ℃) to remove any absorbed moisture. The calcination of the white powder was performed at 200 ℃ for 2 hr in a muffle furnace. Finally, it yielded white and fine un-doped ZnO nanoparticles which were kept at room temperature. The overall chemical reaction of the co-precipitation synthesis method of ZnO NPS is summarized in the Eq. (3.1).

$$Zn(CH_3COO)_2.2H_2O \rightarrow Zn^{2+}{}_{(aq)} + 2CH_3COO_{(aq)}{}^{-} + 2H_2O$$

$$Zn^{2+}{}_{(aq)} + 2OH^{-}{}_{(aq)} \rightarrow Zn(OH)_{2(s)}$$

$$Zn(OH)_{2(s)} \rightarrow ZnO_{(s)} + H_2O_{(g)} \quad (3.1)$$

For the synthesis of $Zn_{0.98}Mn_{0.02}O$ nanoparticle, the amount of manganese acetate dihydrate (Mn $(CH_3COO)_2$. $2H_2O$) used was determined according to the technique already developed using Eq. (2.18) [8].

$$weight\% Mn(CH_3COO)_2.2H_2O = \frac{weight(Mn(CH_3COO)_2.2H_2O)}{weight(Mn(CH_3COO)_2.2H_2O) + weight(Zn(CH_3COO)_2.2H_2O)} x100\% \quad (3.2)$$

Hence, 0.54 g of manganese acetate was dissolved in 100 ml of deionized water and it was mixed with an aqueous zinc acetate dihydrate solution (which was prepared by dissolving 21.95 g of zinc acetate in 100 ml of deionized water). The 0.2 M of aqueous NaOH solution was added drop by drop to the above homogenous mixture to get a white precipitate with pale green color and then similar the above procedure was followed.

Similarly, for the synthesis of $Zn_{0.98}Gd_{0.02}O$ nanoparticle, the amount of Gadolium hexahydrate ($Gd(CH_3COO)_3.6H_2O$) used was determined according to the technique already developed using the Eq. (2.19) [8].

$$weight\%\, Gd(CH_3COO)_3.6H_2O = \frac{weight(Gd(CH_3COO)_2.6H_2O)}{weight(Gd(CH_3COO)_2.2H_2O) + weight(Zn(CH_3COO)_2.2H_2O)} X100\%$$

(3.3)

So, 0.5478 g of Gadolium hexahydrate was dissolved in ethanol-Di water (50–50%) and it was mixed with an aqueous zinc acetate dihydrate solution (which was prepared by dissolving 21.95 g of zinc acetate in 100 ml of deionized water). Then, we followed the same previous procedure [8, 52].

3.4 Determination of antimicrobial activity of ZnO NPs

The antimicrobial properties of the synthesized undoped, Mn-doped and Gd-doped ZnO nanoparticles were investigated by using the Agar well diffusion method of Midaksa et al [1]. The antimicrobial activity determination was against 4 bacteria species (*S. aureus. Bacillus subtilis*, P.aeruginosa, *E. coli*) and fungus (*C. albicans*). These species were cultured in Biology Department of Adama science and Technology University. Staphylococcus aureus (S. aureus). and Bacillus subtilis (B. subtitles) represented Gram-positive bacteria while E. coli and P.aeruginosa represented Gram-negative bacteria. Dimethly sulfoxide was used as negative control for the bacterial strains while bacteriological Gentamicin was used as standard antibiotic for positive control. The strains were transferred to nutrient broth and incubated to grow aerobically at 37 °C for 24 h until it achieved the turbidity of 0.5 McFarland standards. 0.01 mL of each sub-cultured bacteria and yeast test organisms were spread plated using sterilized cotton swab on 20 mL of sterilized molten and cooled MHA media and TSA media, respectively. Subsequently, agar wells of 5 mm diameter were prepared on different plates with sterilized stainless steel cork borer and labeled properly. Solutions of undoped ZnO, Mn and Gd doped ZnO nanoparticles were prepared by dissolving them in Dimethyl sulfoxide (DMSO). Different concentrations (100 $\frac{mg}{\mu L}$, 150 $\frac{mg}{\mu L}$ and 200$\frac{mg}{\mu L}$) of ZnO were added into well using micropipette. The plates containing the microbes and ZnO nanoparticles were incubated at 37 °C for 24 h in case of bacteria and at 28 °C for 48 h in case of yeas. The plates were examined for evidences of zones of inhibition, which appear as a clear area around the wells. The diameter of such zones was measured using ruler and mean value for each organism recorded and expressed in

millimeter and the results were compared with those obtained for the standard drug (Gentamin). For the reference antibiotic, 1 mg was used in the present study. All experiments were performed three times and the results were averaged [1, 38].

3.5. Characterization Techniques

3.5.1 X-ray diffraction (XRD)

X-ray diffractometer (PANalytical XPERT-PRO Diffractometer) with Cu-Kα radiation (λ=1.54056 A^o) and operates at a voltage of 40 kV and current of 30 mA for angle between $2\theta = 10^o \leq 2\theta \leq 80^o$ was used to record the X-ray diffraction (XRD) patterns of undoped, Mn and Gd-doped ZnO nanoparticles and study their crystalline phase. Wurtzite lattice parameters such as the values of interplanar spacing (d), a, c, the dislocation density (δ), the micro-strain (ε) the volume (V) of the unit cell for hexagonal system, the bond lengths (L), the positional parameter (u) and average crystallite size (D) of undoped and doped ZnO nanoparticles were calculated by using Eqs.(2.1- 2.10) [8].

3.5.2 Scanning electron microscopy

The morphology of the NPs was studied using a scanning electron microscope (Hitachi, H 7600). In SEM characterization, nanoparticle powder was mounted on a sample holder followed by coating with a conductive metal. The samples were then scanned with focused fine beam of electrons. The surface characteristics of the sample were obtained from the secondary electrons emitted from the sample surface [53].

3.5.3 UV-Vis absorption spectroscopy

The optical characterization of ZnO NPs was carried out using UV-VIS Spectroscopy. The optical absorption measurements were carried out using UV-Vis absorption spectrophotometer (Perkin Elmer, Lambda 950) in the wave length region of 200 nm -700 nm. First 0.01 g of undoped and doped ZnO nanoparticles was dissolved in 10 ml of dimethyl sulfoxide (DMSO). Then a dimethyl sulfoxide solvent was inserted in a 1 cm cuvette place of the zinc oxide nanoparticles. Next the dimethyl sulfoxide solution was replaced by the zinc oxide nanoparticle solution. After that, the UV-vis absorption spectra was measured and collected. From UV-vis spectra the optical band gaps of pure and doped ZnO NPs were calculated using Eq. (2.17) [51, 54].

4. Results and discussion

In this chapter, the results and discussion of the thesis are presented. In the first section of this chapter, average crystallite size, lattice parameters, micro-strains, dislocation densities, unit cell volumes, bond lengths and positional parameters of ZnO NPs by X-ray diffraction are presented. In section two of this chapter, SEM image of ZnO NPs is presented. In section three, the UV-Vis absorption spectrum and calculated band gaps of ZnO NPs are presented. In section four, antimicrobial activity of ZnO, $Zn_{0.98}Mn_{0.02}O$ and $Zn_{0.98}Gd_{0.02}O$ NPs is presented. All the characterization data were drawn by using origin 6 Software.

4.1 X-ray diffraction (XRD) analysis

The structural analyses of pure, doped ($Zn_{0.98}Mn_{0.02}O$ and $Zn_{0.98}Gd_{0.02}O$) ZnO nanoparticles calcined at 200 °C were carried out using X-ray diffractometer (XRD) and their XRD patterns are depicted in Figure 4.1 (a- c).

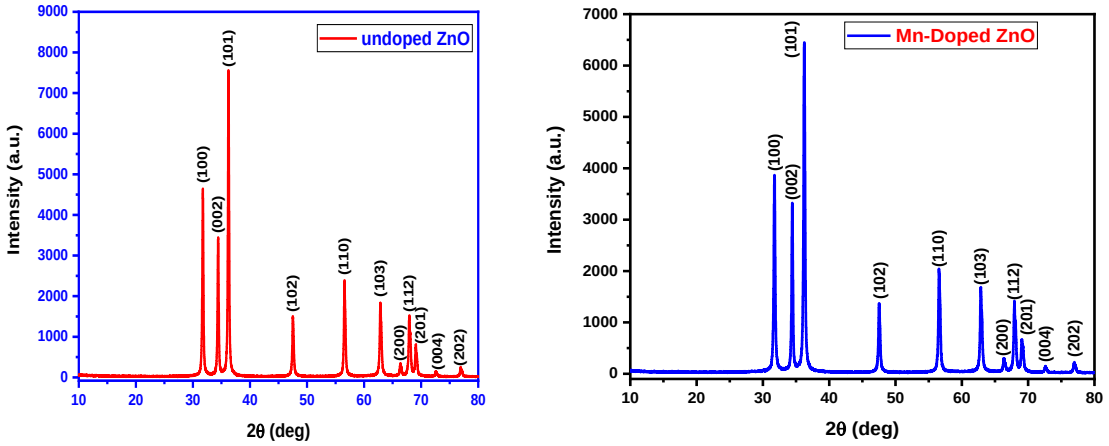

Figure 4.1(a-b): X-ray diffraction patterns of (a) ZnO, (b) $Zn_{0.98}Mn_{0.02}O$ NPs

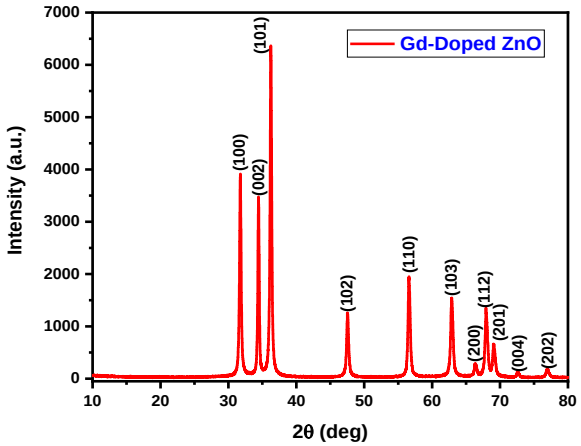

(c)

Figure 4.1 (c): X-ray diffraction pattern of $Zn_{0.98}$ Gd $_{0.02}$ O NP

The diffraction peaks observed at 2θ=31.7480^o, 34.4191^o, 36.2366^o, 36.6165^o, 47.5244^o, 56.5660^o, 56.8454^o, 62.8533^o, 66.3569^o, 67.9250^o, 69.0605^o and 76.9425^o are indexed to (100), (002), (101), (102), (110), (103), (200), (112), (201), (004) and (202) planes, respectively. These diffraction peaks are the characteristics peaks of ZnO. All the observed peaks are attributed to wurtzite structure of ZnO as compared to JCPDS file for ZnO (JCPDS Card No. 00-001-1136) with space group P63mc and lattice parameters a=b= 3.25 A^o and c= 5.206 A^o which is in good agreement with previous report literature [55,56]. From the sharp and high diffracted intensity of X-rays for pure ZnO, it is clear that all the particles exhibit good crystalline nature. The XRD patterns for Mn and Gd-doped samples were found to be exactly the same as that for pure ZnO NPs and similar pattern was observed by other researcher [57].

The XRD result also indicate that no peaks correspond to Mn and Gd as well as MnO and Gd_2O_3 were observed in the XRD pattern confirmed that Mn^{+2} and Gd^{+3} ions have substitutionally replaced the Zn^{2+} without introducing any impurities into the ZnO host lattice. On the other hand, the incorporation of Mn and Gd ions into ZnO host lattice or the replacement of Zn ions by Mn and Gd ions results in the decrement of the intensity of (101) peak which depicts that the degree of crystallinity of samples decreases where as concentration of the defects in the sample increases [58].

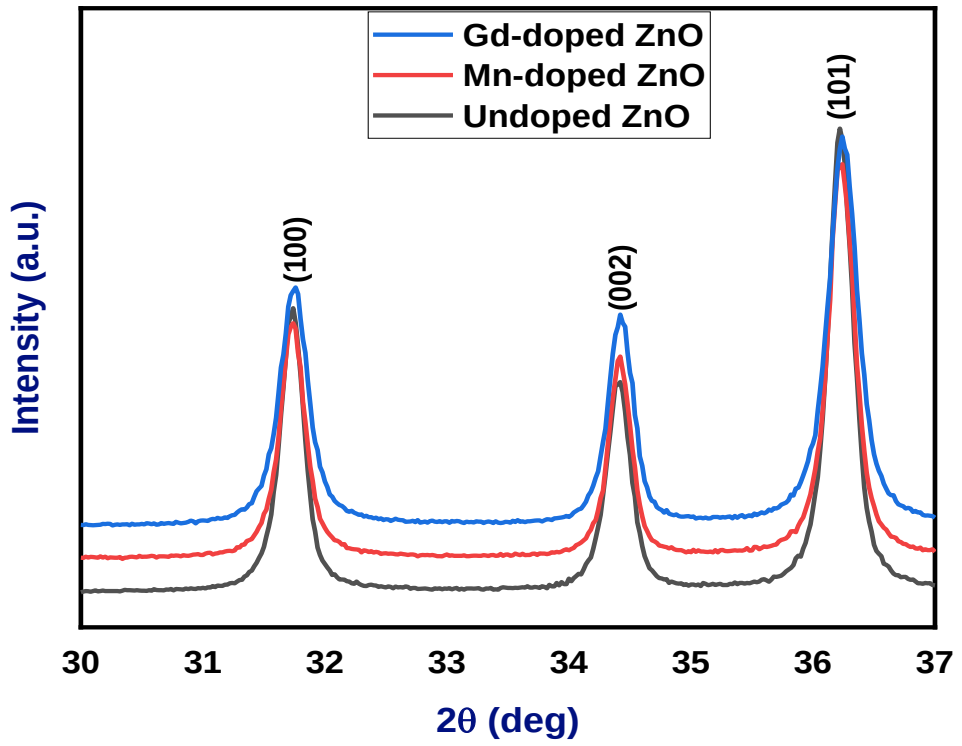

Figure 4.2: Shift analysis for (100), (002) and (1 0 1) peaks of ZnO, $Zn_{0.98}Mn_{0.02}O$ and $Zn_{0.98}Gd_{0.02}O$

The phase shift analyses for (100), (002) and (1 0 1) peaks in the XRD patterns are shown in Figure 4.2. It is clearly seen that the FWHM of the reflection peaks slightly increases after adding the Mn and Gd dopant cations compared to the un-doped ZnO-NPs, indicating the constrain growth of the crystalline or changes in the crystal strains according to the theory stated. Additionally, for $Zn_{0.98}Mn_{0.02}O$ and $Zn_{0.98}Gd_{0.02}O$ nanoparticles, the (100), (002) and (1 0 1) peaks slightly shift towards higher angle compared to undoped ZnO. The (100) peak is shifted from $2\theta = 31.7480^{o}$ to 31.7506^{o} for $Zn_{0.98}Mn_{0.02}O$ and to 31.7604^{o} for $Zn_{0.98}Gd_{0.02}O$ respectively. Similarly, the (002) peak is shifted from $2\theta = 34.4191^{o}$ to 34.4304^{o} for $Zn_{0.98}Mn_{0.02}O$ and to 34.4359^{o} for $Zn_{0.98}Gd_{0.02}$. In the case of (101), it is shifted from $2\theta = 36.2366^{o}$ to 36.2419^{o} and 36.2532^{o} for $Zn_{0.98}Mn_{0.02}O$ and $Zn_{0.98}Gd_{0.02}O$ respectively. Such shifting of the XRD peaks depicts a lattice contraction and is attributed to the strain of the

compound and mismatch of the ionic radii of Gd^{3+} (1.95 A^o), Mn^{2+} (0.66 A^o) and Zn^{2+} (0.74 A^o) or replacement of some Zn cations with Mn and Gd ions in each compound [59].

In addition, the shift in the diffraction peaks is ascribed to the decrease in the crystallite size after the doping of Gd and Mn into the ZnO host lattice which results in the replacement of Zn ion with Gd and Mn ions and the formation of compression stresses in the ZnO that cause the positive shift of the ZnO peak. The positive shift indicates that when Gd and Mn are introduced into ZnO matrix, the lattice contracts and the lattice parameter decreases. Thus, the positive peak shift is an indicator of incorporation of Mn and Gd dopants into the Zn sites [57].

The average crystallite size of the prepared nanoparticles is estimated by using Scherrer formula of Eq. (2.10) with most intense diffraction peak of ZnO (1 0 1). The average crystallite size of pure ZnO NPs is found to be 38 nm. The average crystallite size for Mn and Gd doped ZnO NPs decreases when compared to pure ZnO NPs as shown in Table 4.1. It is observed that the FWHM of the fingerprint diffraction peak of ZnO (1 0 1) increases with Mn and Gd dopants; consequently, the size of nanoparticles decreases as given in Table 4.1, which is in agreement with similar results reported in literature. The decrease in the crystallite size is attributed to the decrease in nucleation and growth of ZnO nanoparticles with the doping [60].

Table 4.1 Average Crystallite size of undoped ZnO, $Zn_{0.98}Mn_{0.02}O$ and $Zn_{0.98}Gd_{0.02}O$ estimated using most intense diffraction peak (1 0 1) of ZnO

Sample	2θ(°)	FWHM(°)	Average Crystallite size [nm]
Pure ZnO	36.2366	0.21940	38
$Zn_{0.98}Mn_{0.02}O$	36.2419	0.22690	36
$Zn_{0.98}Gd_{0.02}O$	36.2532	0.26650	31

The values of lattice parameters (a, c), unit cell volume, bond length and positional parameter are calculated using Eqs. (2.3-2.9) respectively and tabulated in the Table 4.2. It is observed that the unit cell volume, lattice parameters and the bond length slightly decreased after Mn and Gd doping which might result from the difference in the ionic radii of Zn^{2+}, Mn^{2+} and Gd^{3+} (0.74 A^o,

0.66 A^o and 1.95 A^o) respectively. The smaller ionic radius of Mn^{2+} than Zn^{2+} results in the decrement of lattice parameter values of 'a' and 'c' whereas for larger ionic radius of Gd^{3+} than Zn^{2+} the increment of lattice parameter values of 'a' and 'c' of Gd doped ZnO would be expected but decreased due to strain as shown in Table 4.3. This slight variation in the lattice parameters of ZnO, $Zn_{0.98}Mn_{0.02}O$ and $Zn_{0.98}Gd_{0.02}O$ is due to the substitution of Gd and Mn ions with different ionic radii. The slight variation in the aspect ratio (c/a) suggests that the Mn and Gd dopant ions are well substituted into the ZnO crystal lattice and also indicated that the hexagonal wurtzite structure of ZnO is not altered by Mn and Gd dopant ions [57]. The volume of the unit cell of doped ZnO NPs is decreased due to decrement of the lattice parameters after doping. The values calculated values are 47.61$(A^\circ)^3$, 47.30 $(A^\circ)^3$ and 47.01 $(A^\circ)^3$ for ZnO, $Zn_{0.98}Mn_{0.02}O$ and $Zn_0.9_{80}Gd_{0.02}O$ respectively. This indicates that the addition of dopant ions into host lattice occupy partially in tetrahedral Zn positions. There is a strong correlation between c/a ratio and 'u'. In this study, the c/a ratio reveals small perturbation for Mn and Gd doped ZnO NPs. The values of c/a and 'u' parameters are given in Table 4.2 [8].

Table 4.2 Lattice parameters, cell volume and bond length of pure ZnO, $Zn_{0.98}Mn_{0.02}O$ and $Zn_{0.980}Gd_{0.02}O$ nanoparticles.

S.No	Samples	Lattice Parameters (A°) a	c	(c/a)	Volume (V) $(A^o)^3$	Positional parameter (u)	Bond length (Zn–O) (L) (A^o)
1	Pure	3.25	5.206	1.601	47.61	0.379	1.979
2	Mn/ZnO	3.24	5.204	1.606	47.30	0.379	1.973
3	Gd/ZnO	3.23	5.202	1.600	47.01	0.379	1.968

Moreover, the substitution of Mn and Gd ions results in significant changes in Zn–O bond length. From the above table 4.2, it is observed that the Zn–O bond length of pure ZnO NP is 1.979 A°. The bond length values decreased with Mn and Gd-doped ZnO samples due to the replacement of Zn^{2+} ions in ZnO lattice [61].

The reduction in the crystallite size is due to the distortion in a host ZnO lattice by the incorporation of foreign impurities and the presence of Mn^{2+} and Gd^{3+} into host lattice sites hinders the nucleation and subsequent growth rate of ZnO NPs. The substitution of Mn^{2+} and

Gd^{3+} ions in the interstitial position of host ZnO lattice sites influences the concentration of the interstitial Zn, oxygen and Zn vacancies. The detection of small changes in 2θ values and peak broadening of diffraction peaks are due to the increase of micro-strain and line broadening effect caused by size and micro-strain of nanoparticles. The dislocation densities and Microstrain of ZnO NPs were calculated from the Eqs. (2.5) and (2.6), respectively and it is given in the table 4.3 [62]. Comparably, the micro-strain values increase for Mn^{2+} and Gd^{3+} doped ZnO NPs due to the relaxation of strain in the respective unit cells which alter the size and shape of the particles [63].

Table 4.3 Dislocation densities and micro-strain of undoped ZnO, $Zn_{0.98}Mn_{0.02}O$ and $Zn_{0.98}Gd_{0.02}O$ nanoparticles.

Samples	Dislocation density (lines/m^2)	Microstrain x 10^{-4}
Pure ZnO	6.9252E+14	7.72
$Zn_{0.98}Mn_{0.02}O$	7.7160E+14	7.98
$Zn_{0.98}Gd_{0.02}O$	1.0405E+15	9.37

4.2 Scanning Electron Microscopy (SEM) analysis

The morphologies of prepared undoped, Mn- and Gd-doped ZnO nanoparticles were studied using SEM images. Figure 4.3 (a-c) shows the morphologies of ZnO, $Zn_{0.98}Mn_{0.02}O$ and $Zn_{0.98}Gd_{0.02}O$ NPs.

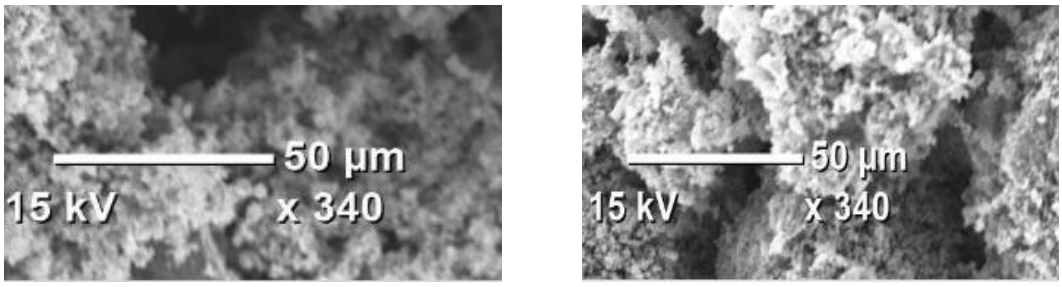

(a) (b)

Figure 4.3 (a-b): SEM images of (a) Undoped ZnO, (b) $Zn_{0.98}Mn_{0.02}O$ NPs

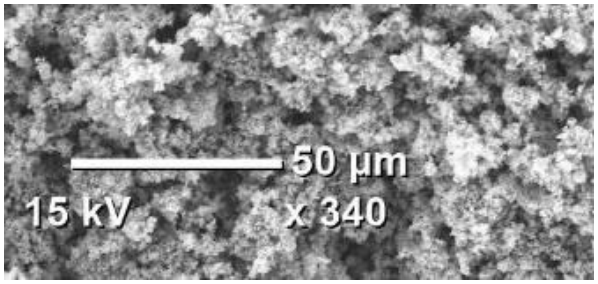

(c)

Figure 4.3 (c): SEM image of $Zn_{0.98}Gd_{0.02}O$ NP.

The particle agglomeration as well as narrow particle size distribution is observed in all of the samples. SEM images show spherical shaped well defined particles [63].

4.3 UV-vis Spectroscopy analysis

The effect of Mn and Gd doping on the optical properties of the samples was investigated by UV-Vis spectrophotometer and the ultraviolet-visible absorption spectra of ZnO, $Zn_{0.98}Mn_{0.02}O$ and $Zn_{0.98}Gd_{0.02}O$ Nanoparticles are shown in Figure 4.4 (a)-(c) respectively.

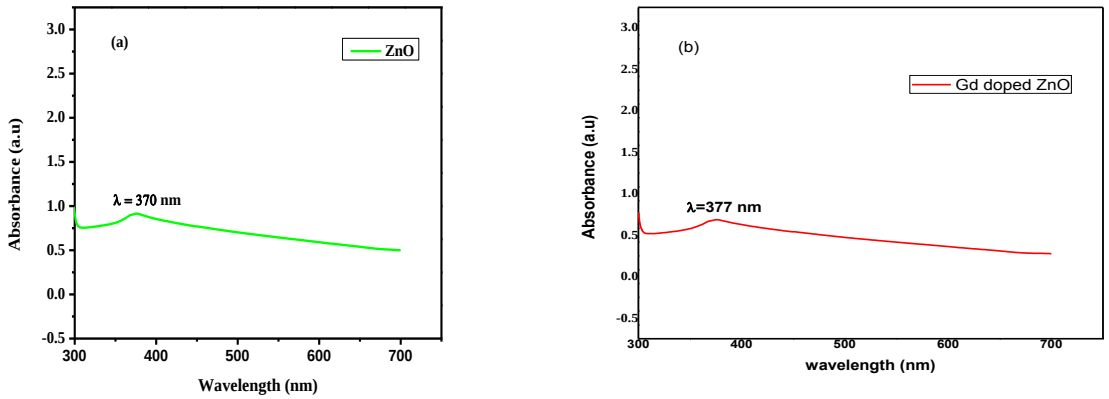

Figure 4.4 (a-b): The ultraviolet-visible absorption spectra of (a) ZnO, (b) $Zn_{0.98}Gd_{0.02}O$ NPs

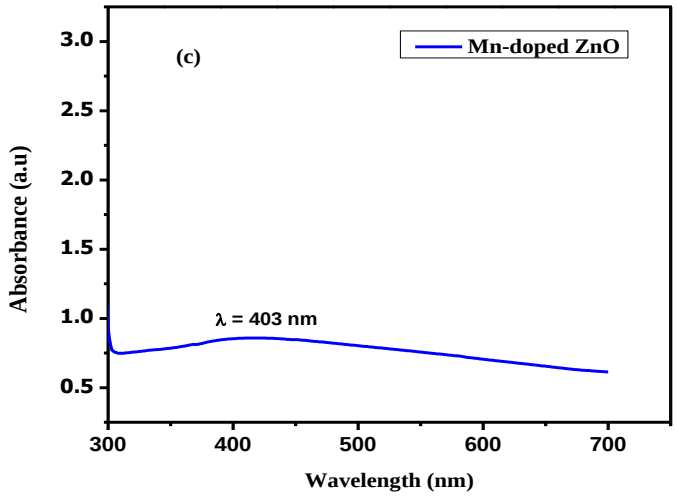

Figure 4.4 (c): The ultraviolet-visible absorption spectra of $Zn_{0.98}Mn_{0.02}O$ Nanoparticle

Table 4.4 Calculated energy band gap of ZnO, $Zn_{0.98}Gd_{0.02}O$ and $Zn_{0.98}Mn_{0.02}O$

Sample	Band gap [eV]
Pure ZnO	3.35
$Zn_{0.98}Gd_{0.02}O$	3.28
$Zn_{0.98}Mn_{0.02}O$	3.07

The strongest absorption peaks are seen at 370 nm, 377 nm and 403 nm for undoped Zno, $Zn_{0.98}Gd_{0.02}O$ and $Zn_{0.98}Mn_{0.02}O$ respectively. The corresponding optical band gap energy calculated using Eq. (2.17) was found to be in the range of 3.07-3.35 eV and it is given in the Table 4.4 above. The absorption peaks are in the ultraviolet regions and originate from the transition of electron from valence band (VB) to conduction band (CB) [64]. It is observed that undoped ZnO NP exhibited blue shifted absorbance peak as compared to its bulk counterpart having absorbance peak at 386 nm (3.2 eV) at room temperature. On another hand, we observed the decrement of the energy band gap of ZnO NPs with the doping of Mn and Gd ions and this shift is ascribed to the influence of dopant ions. The interaction of d electron of Mn ion and f electron of Gd ion with sp electron of ZnO may cause the dopant induced states within the energy gap of ZnO NPs. These states correspond to the dopant provide additional pathways for electronic transition, thus giving rise to the red shift of absorption that is a slight shift of UV

peak towards the longer wavelength side is found with the incorporation of Mn^{2+} and Gd^{3+} ions into ZnO matrix [66].

4.4 Antimicrobial Studies

Figure 4.5 (a-e) shows the zones of inhibition of pure ZnO, $Zn_{0.98}Mn_{0.02}O$ and $Zn_{0.98}Gd_{0.02}O$ nanoparticles against different pathogens (P. aeruginosa, E. coli, S. aureus, B. subtillis and C.albicans) with different concentrations (100 $\frac{mg}{\mu L}$, 150 $\frac{mg}{\mu L}$ and 200 $\frac{mg}{\mu L}$). It was carried out using agar well diffusion method to observe their ability as a potential antimicrobial agent.

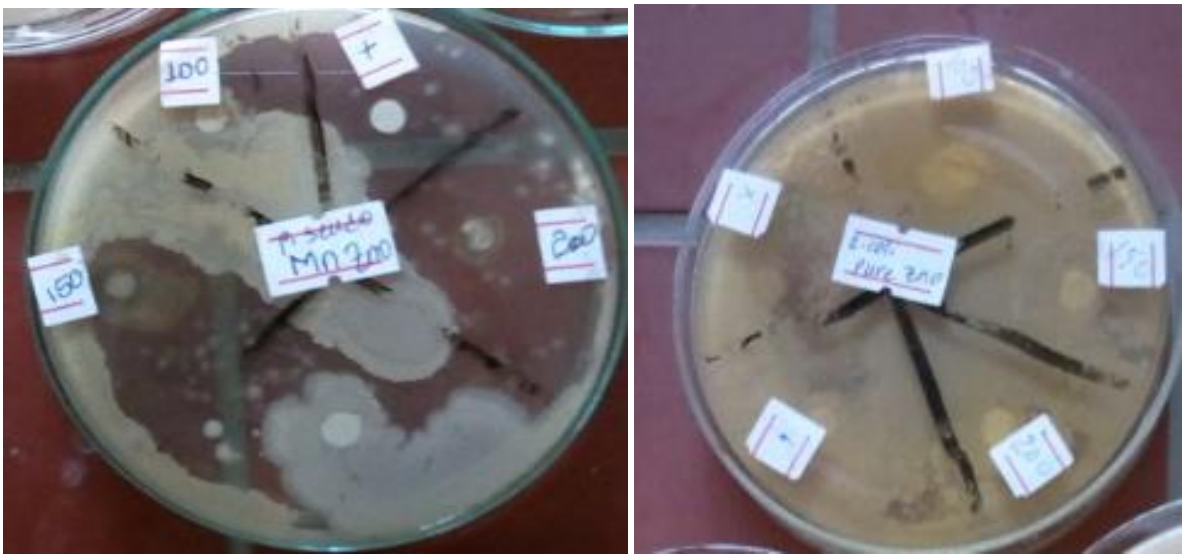

(a) (b)

Figure 4.5 (a-b): The antimicrobial activity of (a) $Zn_{0.98}Mn_{0.02}O$ NP applied on P. aeruginosa (b) pure ZnO NP applied on E. coli with different concentrations (100 $\frac{mg}{\mu L}$, 150 $\frac{mg}{\mu L}$ and 200 $\frac{mg}{\mu L}$)

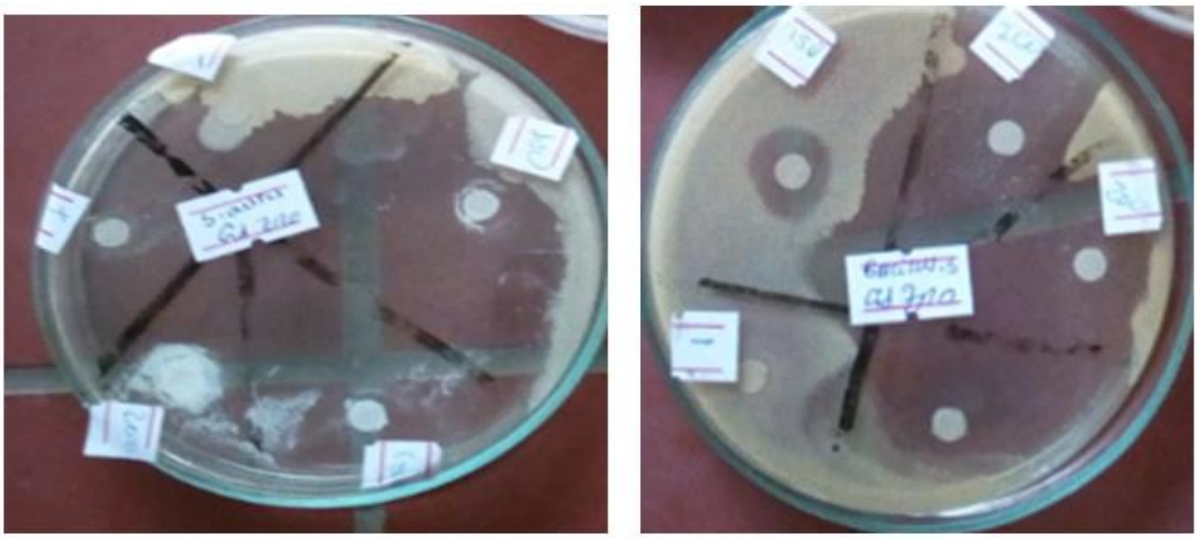

(c) (d)

Figure 4.5 (c-d): The antimicrobial activity of $Zn_{0.98}Gd_{0.02}O$ NP applied on (c) S. aureus (d) B. subtillis with different concentrations (100 $\frac{mg}{\mu L}$, 150 $\frac{mg}{\mu L}$ and 200 $\frac{mg}{\mu L}$)

(e)

Figure 4.5 (e): The antimicrobial activity of $Zn_{0.98}Gd_{0.02}O$ NP applied on C.albicans with different concentrations (100 $\frac{mg}{\mu L}$, 150 $\frac{mg}{\mu L}$ and 200 $\frac{mg}{\mu L}$)

The antimicrobial activity of pure, Mn doped and Gd doped ZnO NPs nanoparticles are attributed to the release of Zn^{2+}, Mn^{2+} and Gd^{3+} ions in dissolution as well as the electrostatic attraction between negatively charged bacterial cells and positively charged nanoparticles, internalization into the bacterial cell wall and formation the reactive oxygen species (ROS) generation such as H_2O_2, hydroxyl radical (OH^-), superoxide anion radical (O_2^-) ,which cause damage to intracellular components such as DNA and cellular proteins, and may even lead to cell death [66,67].

The results obtained to show the effects of concentrations on the antimicrobial activity of ZnO NPs are illustrated in Table (4.5-4.7) and Figure 4.6 (a-c). In this study, different concentrations (100 $\frac{\mu g}{mL}$, 150 $\frac{\mu g}{mL}$ and 200 $\frac{\mu g}{mL}$) of nanosized pure ZnO, Mn- and Gd-doped ZnO NPs were tested on different pathogens. All experiments were performed three times and the results were averaged.

Table 4.5 Zones of inhibition of ZnO, $Zn_{0.98}Mn_{0.02}O$ and $Zn_{0.98}Gd_{0.02}O$ on different types of pathogens with concentration of 100 $\frac{\mu g}{mL}$

Types of Pathogens	Zones of inhibition (mm) of 100 $\frac{\mu g}{mL}$ of NPs			
	ZnO	$Zn_{0.98}Mn_{0.02}O$	$Zn_{0.98}Gd_{0.02}O$	Gentamicin (+ control)
E. coli	NZ	5±0.1	18±0.4	19±0.21
P. aeruginosa	NZ	4±0.4	15±0.5	17±0.13
B. subtillis	5±0.12	10±1.1	20±0.2	28±0.43
S. aurues	2±0.4	15±1.2	19±0.1	29±0.32
C. albicans	NZ	10±0.2	15±1.3	21±0.51

Note: NZ= No Zone

Table 4.6 Zones of inhibition of ZnO, $Zn_{0.98}Mn_{0.02}O$ and $Zn_{0.98}Gd_{0.02}O$ on different types of pathogens with concentration 150 $\frac{\mu g}{mL}$

Types of Pathogens	Zones of inhibition (mm) of 150 $\frac{\mu g}{mL}$ of Nps			
	ZnO	$Zn_{0.98}Mn_{0.02}O$	$Zn_{0.98}Gd_{0.02}O$	Gentamicin (+ control)
E. coli	NZ	10±0.1	20±0.3	19±0.21
P. aeruginosa	NZ	10±0.4	15±0.15	17±0.13
B. subtillis	7±0.13	17±1.0	25±0.2	28±0.43
S. aurues	3±0.1	20±0.2	25±0.1	29±0.32
C. albicans	NZ	10±1.2	20±1.1	21±0.51

Table 4.7 Zones of inhibition of ZnO, $Zn_{0.98}Mn_{0.02}O$ and $Zn_{0.98}Gd_{0.02}O$ on different types of pathogens with concentration 200 $\frac{\mu g}{mL}$

Types of Pathogens	Zones of inhibition (mm) of 200 $\frac{\mu g}{mL}$ of NPs			
	ZnO	$Zn_{0.98}Mn_{0.02}O$	$Zn_{0.98}Gd_{0.02}O$	Gentamicin (+ control)
E. coli	NZ	10±0.2	20±1.3	19±0.21
P. aeruginosa	NZ	10±0.5	15±0.6	17±0.13
B. subtillis	10±0.1	18±1.4	30±0.3	28±0.43
S. aurues	7±0.3	22±1.2	29±0.4	29±0.32
C. albicans	2±0.12	18±1.3	21±1.11	21±0.51

Note: NZ= No Zone

It is observed that the antimicrobial activity of ZnO nanoparticles increase with the concentrations due to the increment of reaction between oxygen and dehydrogenase enzyme which enhances antimicrobial activity as shown in Figure 4.6(a-c).

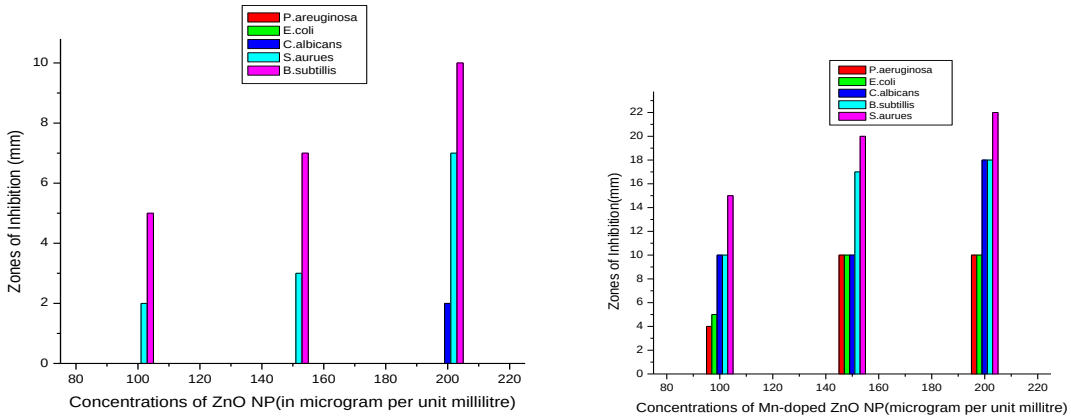

(a) (b)

Figure 4.6 (a-b): The antimicrobial activities of undoped and Mn-doped ZnO NPs applied against gram positive bacteria (S.aurues and B.subtillis), gram negative bacteria (E.coli and P.aeruginosa) and fungus (C.albicans) different concentrations (100 $\frac{\mu g}{mL}$, 150 $\frac{\mu g}{mL}$ and 200 $\frac{\mu g}{mL}$ **).**

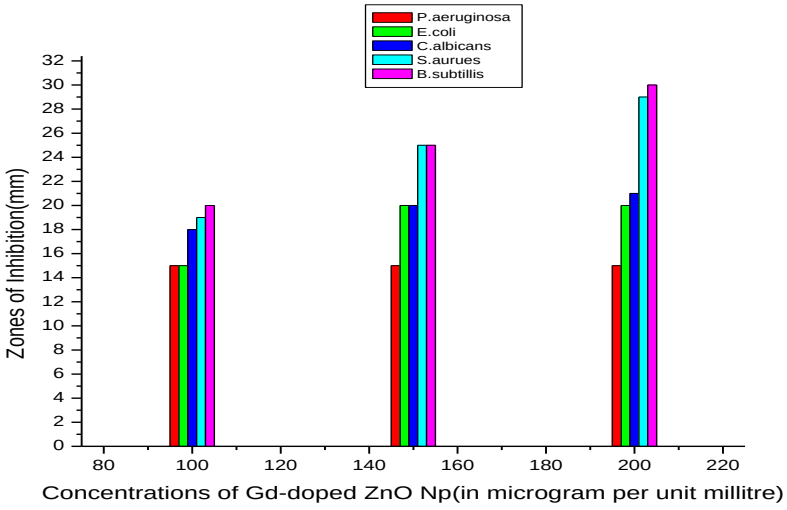

(c)

Figure 4.6 (c): The antimicrobial activities of Gd -doped ZnO NP applied against gram positive bacteria (S.aurues and B.subtillis), gram negative bacteria (E.coli and P.aeruginosa) and fungus (C.albicans) different concentrations (100 $\frac{\mu g}{mL}$, 150 $\frac{\mu g}{mL}$ and 200 $\frac{\mu g}{mL}$ **).**

The interaction between the NPs and the cell wall of bacteria was changed due to doping of Mn and Gd. The doping of Mn and Gd with ZnO may lead to the variation in grain size, optical, morphology, and solubility of Zn^{2+} ions. All these factors combined together have a significant effect on the antibacterial activity of ZnO [68-69]. In this study, the antimicrobial activity of ZnO NPs is increased with decreasing size of the crystal and energy band gap. It is observed that $Zn_{0.98}Gd_{0.02}O$ showed better antimicrobial activity than $Zn_{0.98}Mn_{0.02}O$ and undoped ZnO due to its small size as shown in Figure 4.7.

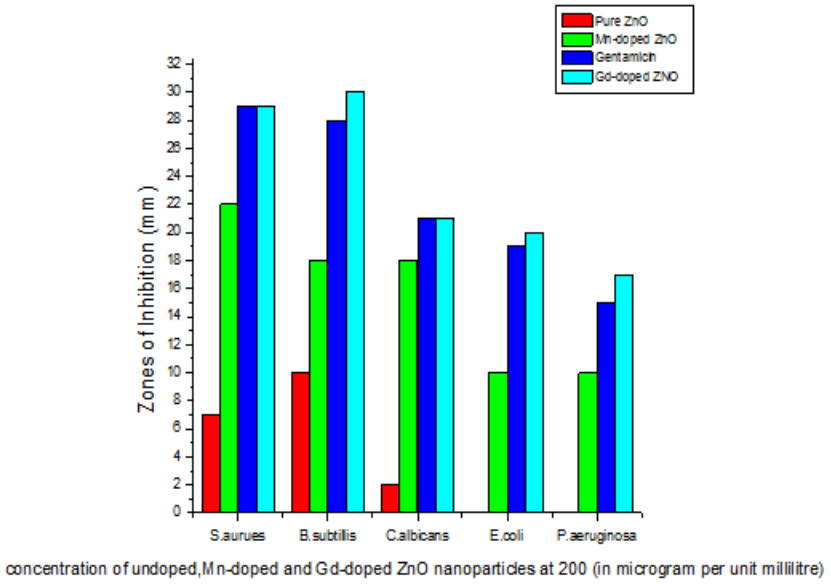

Figure 4.7: The antimicrobial activities of undoped, Mn and Gd doped ZnO NPs and Gentamicin drug against gram positive bacteria (S.aurues and B.subtillis), gram negative bacteria (E.coli and P.aeruginosa) and fungus (C.albicans) at the concentration of 200 $\frac{\mu g}{mL}$.

It showed that smaller size particles enhanced antimicrobial activity due to the larger surface area to volume ratio [70]. The growth of all bacteria and fungus were more highly affected by Gd^{3+} - and Mn^{2+} -doped ZnO nanostructures compared with pure ZnO NPs. The other reason of increment of antimicrobial activity of Gd doped ZnO NPs is ascribed to large generation of ROS species as doping creates a large number of defects which increases ROS species and consequently the antimicrobial activity. Generally, nanoparticles with better photocatalytic activity have larger specific surface areas and smaller crystallite sizes, which increase oxygen vacancies, resulting in more ROS. Furthermore, due to the various surface-

interface characteristics may have different chemical-physical, adsorption-desorption abilities in the direction towards bacteria, make sure in different antibacterial performances. The results have revealed that Gd and Mn-doped ZnO nanostructures will be a promising candidate to be used for potential drug delivery systems to cure some significant infections in the near future [71,72].

In the present study, we found that gram-positive bacteria were more sensitive than gram-negative bacterial strains and fungus against the NPs tested. All ZnO, Mn and Gd-doped ZnO NPs were more sensitive to *S. aureus* and *E. coli* as shown in Figure 4.7. Positive activities of ZnO, Mn and Gd-doped ZnO NPs against gram-negative bacteria and fungus were also observed. More activity towards gram-positive bacteria is ascribed to the difference in their structure and chemical composition. The cell wall of gram-positive bacteria has single membrane where as the gram-negative bacteria cell wall has outside and inside cytoplasmic membrane as well as Lippopolysaccride that covers peptidoglycan. So, in the case of gram-positive bacteria the electrostatic interactions between NPs and cell surface results in more destruction and cell death than gram-negative bacteria. It was also reported earlier that various bacterial strains had considerably different infectivity and tolerance levels towards the different agents including antibiotics. Also differences in the antibacterial activity might be due to different particle dissolution. [73]

5. Conclusions

Undoped, Mn doped and Gd doped ZnO nanoparticles were successfully synthesized via chemical co-precipitation method by using zinc acetate, Manganese acetate, Gadolium acetate as a precursors; sodium hydroxide as precipitating agent and distilled water and ethanol as solvents. The effects of Mn and Gd dopants on structural, morphological, optical properties and antimicrobial activity of ZnO nanoparticles were investigated. The obtained nanoparticles were characterized by XRD, SEM and UV-vis. The XRD result revealed that the synthesized ZnO NPs were in nanometer range with average crystallite size about 31–38 nm from the Scherer's formula. It depicted a single phase of pure, Mn- and Gd-doped ZnO nanoparticles. In addition, the XRD measurement showed that the hexagonal phase of the wurzite structure of ZnO was not disturbed by the Mn and Gd dopants, apart from variations or perturbations in the unit cell dimension. The lattice parameters, unit cell volume and bond length were decreased with the doping of Gd and Mn. On another hand, physical defects and dislocations were increased. It was also perceived that XRD peaks shifted to higher diffraction angles due to the difference of the ionic radii of Mn^{2+} (0.66 A°), Zn^{2+} (0.74 A°) and Gd^{3+} (1.95 A°). The size and morphology of the synthesized nanoparticles confirmed by scanning electron microscopy analysis is that ZnO NPs were successfully prepared. Morphological studies have revealed the formation of spherical nanoparticles for all samples. Optical band gap energy was found to be decreased from 3.35 eV to 3.28 eV and 3.07 eV with Gd and Mn doping respectively, due to the introduction of new energy levels in the energy band gap. The zone of inhibition was observed against pathogenic bacteria and fungus strains and suggests that $Zn_{0.98}Gd_{0.02}O$ and $Zn_{0.98}Mn_{0.02}O$ showed good antimicrobial activity adjacent to gram-positive bacteria (S. aureus and B. subtilis), gram-negative bacteria (E. coli and P. aeruginosa) and fungus (C. albicans) than the undoped ZnO nanoparticles. Also, the results of this study depicted that the antimicrobial activities of synthesized NPs were increased with the concentration and size decrement of the crystal. Furthermore, the results indicated that the gram-positive bacteria were more sensitive to all undoped, Mn- and Gd-doped ZnO NPs than gram-negative bacteria and fungus.

“This research project is funded by Adama Science and Technology University under the grant number ASTU/SM-R/021/19.’’

References

[1] M. Kasahun, A. Yadate, A. Belay, Z. Belay, and M. Ramalingam, Antimicrobial Activity of Chemical, Thermal and Green Route-Derived Zinc Oxide Nanoparticles: A Comparative Analysis. Nano Biomed. Eng., 2020, 12 (1): 47 – 56.

[2] A. Creely, Nanoparticles: An Occupational Hygiene Review. Research Report 274, 2004.

[3] N. Sharma, S. Jandaik, S. Kumar, M. Chitkara, & I. Singh Sandhu, Synthesis, characterisation and antimicrobial activity of manganese- and iron-doped zinc oxide nanoparticles. Journal of Experimental Nanoscience, 2016, 11:1, 54-71.

[4] A. Naskar, S. Lee, and K. Kim, Antibacterial potential of Ni-doped zinc oxide nanostructure: comparatively more effective against Gram-negative bacteria including multi-drug resistant strains. RSC Adv., 2020, 10:1232.

[5] W. O. Gordon, Metal Oxide Nanoparticles: Optical Properties and Interaction with Chemical Warfare Agent Simulants. Dissertation, Blacksburg, Virginia, USA, 2006.

[6] R. Taziwa, E. Meyer, D. katwire, and L. Ntozakle, Influence of Carbon Modification on the Morphological, Structural, and optical properties of Zinc oxide Nanoparticles Synthesized by Pneumatic spray pyrolysis Technique. The Journal of nanoparticles, 2017, 9:11: Article ID 9095301.

[7] P. Tartaj, M. Del Puerto Morales, S. Veintemillas-Verdaguer, T. González-Carreño, and C. J. Serna, The preparation of magnetic nanoparticles for applications in biomedicine. Journal of Physics D: Applied Physics, 2003, 36(13):182–197.

[8] G. Vijayaprasath, R. Murugan, S. Asaithambi, P. Sakthivel, T. Mahalingam, Y. Hayakawa, and G. Ravi, Structural and magnetic behavior of Ni/Mn co-doped ZnO nanoparticles prepared by co-precipitation method. Ceramics International, 2016, 42:2836–2845.

[9] C. Jayachandraiah and G. Krishnaiah, Influence of cerium dopant on magnetic and dielectric properties of ZnO nanoparticles, J Mater Sci.,2019, 8: 45-67.

[10] M. Vaseem, A. Umar, and Y.B. Hahn ZnO Nanoparticles: Growth, Properties, and Applications. American Scientific Publisher, 2010, 5: 1–36.

[11] K. Ranjit, and A. A. Baquee, An overview of preparation, characterization and application of ZnO. Int. Res J of pharm, 2013, 4:47-57.

[12] R. S. Selvakumar, and D. Kumar, Hydrothermal mediated synthesis of ZnO nanorods and their antibacterial properties. Open Access Journal Letters in Applied Nano Bioscience, 2012, 1:002-007.

[13] N. Shakti, and P. S. Gupta, Structural and Optical Properties of Sol-gel Prepared ZnO Thin Film. Applied Physics Research, 2010, 2: 1928.

[14] Z. H. Ibupoto, K. Khun, M. Erksson, M. AlSalhi, M. Atif, A. Ansari, M. Willander, Hydrothermal Growth of Vertically Aligned ZnO Nanorods Using a Biocomposite Seed Layer of ZnO Nanoparticles. Materials, 2013, 6: 3584-3597.

[15] Z. L. Wang, Zinc oxide nanostructures: growth, properties and applications. J. Phys: Condens Matter, 2004, 16(25): 829–858.

[16] Ü. Özgür, Ya. I. Alivov, C. Liu, A. Teke, M. A. Reshchikov, S. Doan, V. Avrutin, S. J. Cho, and H. Morkoç, A comprehensive review of ZnO materials and devices. Journal of Applied Physics, 2005, 98:041301.

[17] S. J. Pearton, D. P. Norton, K. Ip, Y. W. Heo, and T. Steiner, Recent progress in processing and properties of ZnO. Progress in Materials Science, 2005, 50:293-340.

[18] S. Singh et al, Structure, microstructure and physical properties of ZnO based materials in various forms: bulk, thin film and nano. J. Phys. D: Appl. Phys. 2007, 40:6312-6327.

[19] Z. Fan and J. G. Lu, Zinc Oxide Nanostructures: Synthesis and properties. J. Nanosci Nanotechnol., 2005, 5:1561-73.

[20] J. Cui, Zinc oxide nanowires. Materials Characterization, 2012, 64:43-52.

[21] D. Chen, K. Wang, D. Xiang, R. Zong, W. Qa, and Y. Zhu (2014) Significantly enhancement of photocatalytic performances via core-shell structure of ZnO, Journal of applied Catalysis B, Environmental 147: 554-561.

[22] T. D. Malevu, Synthesis of ZnO Nanoparticles using environmentally friendly Zinc Air System. University of the Free State, online thesis, 2015.

[23] G. Ceder, D. Morgan, and C. G. Van de Walle, First-principles study of native point defects in ZnO. Physical Review B, 2000, 61(22): 15019.

[24] H. Morkoc and U. Ozgur, General properties of ZnO, Zinc Oxide: Fundamentals, materials and device technology. WILEY-VCH Verlag, 2009, 8:1-2.

[25] C. Klingshirn, ZnO: From basics towards applications. Phys. Stat. Sol. (b), 2007, 244(9): 3027 -3073.

[26] R. Zhu and R. Yang, Separation of the piezotronic and piezoresistive effects in a zinc oxide nanowire, Nanotechnology, 2014, 25: 345702.

[27] A. Janotti and C. G. Van de Walle, Fundamentals of zinc oxide as a semiconductor. Rep. Prog. Phys., 2009, 72:126501.

[28] A. B. Djurisic, and Y. H. Leung, Optical properties of ZnO nanostructures. Journal of Electronic Materials, 2006, 2(8-9):944-961.

[29] S. J. Pearton, D. P. Norton, M. P. Ivill, A. F. Hebard, J. M. Zavada, W. M. Chen, and I. A. Bunyanova, Ferromagnetism in transition-metal doped ZnO. Journal of Electronic Materials, 2007, 36(4): 462-471.

[30] S. B. Zhang, S. H. Wei, and A. Zunger, The microscopic origin of the phenomenological doping-limit-rule in semiconductors and insulators. Phys. Rev. Lett., 2000, 84:1232.

[31] X. H. Zhang, J. Chen, Y. Wub, Z. Xie, J. Kang, and L. Zheng, A simple route to fabricate high sensibility gas sensors based on erbium doped ZnO nanocrystals. Colloid. Surf. A: Physicochem.Eng. Aspect., 2011, 384:580.

[32] B. Meyer, and D. Marx, Density-functional study of the structure and stability of ZnO surfaces Phys. Rev. B, 2003, 67:035403.

[33] D. Daksh and Y. K. Agrawal, Reviews in Nanoscience and Nanotechnology, 2016, 5: 1–27.

[34] J. Han, F. Fan, C. Xu, S. Lin, M. Wei, X. Duan, and Z. L. Wang, ZnO nanotube-based dye-sensitized solar cell and its application in self-powered devices. Nanotechnol, 2010, 21:405203.

[35] M. Suchea, N. Kornilios, and E. Koudoumas, Zinc oxide films chemically grown on to rigid and flexible substrates for TFT applications. Physica B, 2010, 405: 4389.

[36] I. Kazeminezhad, S. Saadatmand, and R. Yousefi, Effect of transition metal elements on the structural and optical properties of ZnO nanoparticles. Bull. Mater. Sci., 2016, 39(3):719–724.

[37] V. Chiriac, D. N. Stratulat, G. Calin, S. Nichitus, V. Burlui, C. Stadoleanu, M. Popa, and I. M. Popa, Antimicrobial property of zinc based nanoparticles. IOP Conf. Series: Materials Science and Engineering, 2016, 133:012055.

[38] M. Oves, M. Arshad, M. S. Khan, A. S. Ahmed, A. Azam, and M.I. Ismail, Anti-microbial activity of cobalt doped zinc oxide nanoparticles: Targeting water borne bacteria Journal of Saudi Chemical Society, 2015, 19:581-588.

[39] B. L. Silva, M. P. Abuçafy, E. B. Manaia, J. A. Junior, B. G. Chiari-Andréo, R. CL. Pietro, and L. A. Chiavacci, An Overview Relationship Between Structure And Antimicrobial Activity Of Zinc Oxide Nanoparticles. Int J Nanomedicine, 2019, 14: 9395–9410.

[40] B. D. Cullity and S. R. Stock, Elements of X-ray Diffraction. Prentice Hall, Upper Saddle River, NJ, 2001.

[41] E. G. Nental, Principles of Environmental Geochemistry: Brooks/Cole –Thomson learning, 2004:212-214.

[42] A. Nehal, M. Salahuddin, K. Aged, et al., Synthesis and characterization of ZnO nanoparticles via precipitation method: Effect of annealing temperature on particle size. Nanoscience and Nanotechnology, 2015, 5(4):82-88.

[43] R. Jalal, M. Abareshi, E. K. Goharshadi, et al., ZnO nanofluids: green synthesis, characterization and antibacterial activity. Materials Chemistry and Physics, 2010, 121(1-2): 198-201.

[44] http://www.unl_edu/CMRACfem/semoptic.htm. [Accessed 20/10/2016].

[45] http://serc.carleton.edu/research_education/geochemsheets/techniques/SEM.html.[Accessed 20/10/2016].

[46] http://serc.carleton.edu/research_education/geochemsheets/techniques/SEM.html.[Accessed 20/10/2016].

[47] B. K. Meyer, H. Alves, D. M. Hofmann, W. Kriegseis, D. Forster, F. Bertram, J. Christen, A. Hoffmann, M. Straßburg, M. Dworzak, U. Haboeck, and A. V. Rodina, Bound exciton and donor–acceptor pair recombination in ZnO. Phys. Stat. Sol, 2004, 241:231-260.

[48] N. S. Singh, Synthesis, Characterization, Photoluminescence and Magnetic Properties of Zinc Oxide Nanoparticles. Ph. D. Thesis, 2009.

[49] S. Kumar, Spectroscopy of Organic Compounds. Amritsar, 2006:143005.

[50] Z. Chen et al, UV-vis spectroscopy, photoelectrochemical water splitting. Springer Briefs in Energy, 2013:49.

[51] A. J. Ahmed, Effect of transition metal doping on the structural, optical, thermal properties, and antimicrobial activity of zinc oxide nanoparticles. Int. Res. J. Pharm., 2018.

[52] Sh. Jeetendra, H. Nagabhushana, K. Mrudula, C. S. Naveen, P.Raghu, and H. M. Mahesh, Concentration Dependent Optical and Structural Properties of Mo doped ZnTe Thin Films Prepared by e-beam Evaporation Method. Int. J. Electrochem. Sci., 2014, 9:2944 -2954.

[53] W. Zhou, R. Apkarian, Z. L. Wang, and D. Joy, Fundamentals of scanning electron microscopy (SEM), Scanning microscopy for nanotechnology: Techniques and applications. Springer, New York, 2007:1-40.

[54] S. Getie, A. Belay, R.A.R. Chandra, et al.,Synthesis and characterizations of zinc oxide nanoparticles for antibacterial applications. Nanomedicne and Nanotechnology, 2017, S8.

[55] A.B. Gemta, B. Bekele, and A.R.C. Reddy, Effects of temperature and polyvinyl alcohol concentrations in the synthesis of zinc oxide nanoparticles. Digest Journal of Nanomaterials and Biostructure, 2019, 14:51-60.

[56] P. Ghosh and A.K. Sharma, Optical characterization and growth mechanism of combination of zinc oxide nanowires and nanorods at various substrate temperatures. Journal of Nanomaterials, 2013: Article ID 480164, 9.

[57] M. Sarfraz, N. Ahmed, K.U. Haq, SH. SHahida, and M. A. Khana, Structural optical and magnetic properties of transition metal doped ZnO magnetic nanoparticles synthesized by sol-gel auto-combustion method. Materials Science-Poland, 2019, 37(2):280-288.

[58] Y. Abdollahi, A. H. Abdullah, Z. Zainal, and N. A. Yusof, Synthesis and characterization of Manganese doped ZnO nanoparticles. International Journal of Basic & Applied Sciences IJBAS-IJENS, 2015, 11(04).

[59] R. K. Sharma, S. Patel, and K. C. Pargaien, Synthesis, characterization and properties of Mn-doped ZnO nanocrystals. Adv. Nat. Sci.: Nanosci. Nanotechnol., 2012, 3:035005.

[60] M. Aparecida, R. Bonifácio, H. d. L. Lira, L. S. Neiva, and L. Gama, Nanoparticles of ZnO Doped With Mn: Structural and Morphological Characteristics. Materials Research, 2017, 20(4): 1044-1049.

[61] G. Vijayaprasath, G. Ravi, A. S. Haja Hameed, and T. Mahalingam, Effect of cobalt doping on structural, optical, and magnetic properties of ZnO nanoparticles synthesized by coprecipitation method. J. Phys. Chem.C, 2014, 118: 9715.

[62] G. Ravi, T. Mahalingam, and Y. Hayakawa, Characterization of dilute magnetic semiconducting transition metal doped ZnO thin films by sol–gel spin coating method. Appl. Surf. Sci., 2014, 313: 870.

[63] S. D. Senol, B. Yalcin, E. Ozugurlu, and L. Arda, Structure, microstructure, optical and photocatalytic properties of Mn-doped ZnO nanoparticles. Mater. Res. Express, 2020, 7:015079.

[64] J. H. Zheng, J. L. Song, Z. Zhao, Q. Jiang, and J. S. Lian, Optical and magnetic properties of Nd-doped ZnO nanoparticles. Cryst. Res. Technol., 2012, 47(7):713–718.

[65] S. S. Sartiman, N. F. Djaja, R. Saleh, Chromium-Doped ZnO Nanoparticles Synthesized by

Co-Precipitation: Chromium Effects. Materials Sciences and Applications, 2013, 4:528-537.

[66] A. Popa, M. Stan, D. Toloman, S.A. Porav, R. Stefan, D.C. Vodnar, and T.D. Silipas, The influence of cu^{2+} doping level on the properties of ZnO loaded with Ag nanoparticles. Romanian Journal of Physics, 2018, 63:609.

[67] S. Stoleriu, C. Lungu, C. D. Ghitulica, A. Surdu, G. Voicu, A. Cucuruz, C. S. Turculet and L. T. Ciocan, Influence of Dopant Nature on Biological Properties of ZnO Thin-Film Coatings on Ti Alloy Substrate. Nanomaterials, 2020, 10:129.

[68] L. Zhang, Y. Jiang, and M. Ding, Investigation into the antibacterial behavior of suspensions of ZnO nanoparticles (ZnO nanofluids). J. Nanopart. Res, 2007, 9(3): 479-489.

[69] J. Zhang, Silver-coated zinc oxide nano antibacterial synthesis and antibacterial activity characterization. International Conference on Electronics and Optoelectronics (ICEOE), 2011, 3:94-98.

[70] Sh. A. Khan, S. Shahid, W. Bashir, S. Kanwal, and A. Iqbal, Synthesis, characterization and evaluation of biological activities of manganese-doped zinc oxide nanoparticles. Tropical Journal of Pharmaceutical Research October, 2017, 16(10): 2331-2339.

[71] A. F. Fathima, R. J. Mani, K. Sakthipandi, K. Manimala, and A. Hossain, Enhanced Antifungal Activity of Pure and Iron-Doped ZnO Nanoparticles Prepared in the Absence of Reducing Agents. Journal of Inorganic and Organometallic Polymers and Materials, 2019, 13:0123456789.

[72] S. Gunalan, R. Sivaraj, and V. Rajendran, Green synthesized ZnO nanoparticles against bacterial and fungal pathogens. Progress in Natural Science: Materials International, 2012, 22(6):693-700.

[73] Z. E. Karvani and P.Chehrazi, Antibacterial activity of ZnO nanoparticles on gram positive and gram-negative bacteria. African Journal of Microbiology Research, 2011, 5(2): 1368-1373.